CHAPTER 5

CHARACTERIZATION OF CURCUMIN-ENRICHED PICKERING NANOEMULSION STABILIZED WITH NANOCELLULOSE SYNTHESIZED FROM COCONUT MILK RESIDUE

Chapter 5

Characterization of curcumin-enriched Pickering nanoemulsion stabilized with nanocellulose synthesized from coconut milk residue

5.1 Introduction

In comparison to conventional cellulose materials, nanocellulose exhibits several remarkable properties, including high specific surface area, high aspect ratio, low density, minimal thermal expansion, strong mechanical and optical properties, and high chemical reactivity. Cellulose nanostructures are isolated using a variety of top-down strategies, including solvent-assisted isolation, cryocrushing, ultra-fine friction grinding, high pressure homogenising, acid hydrolysis, ultrasound, enzyme-assisted hydrolysis, and 2,2,6,6-tetramethylpiperidine-1-oxyl (TEMPO) mediated oxidation. The application of nanocellulose depends on its form and characteristics (Yang et al., 2017). Acid hydrolysis and chemical/mechanical disintegration yield CNFs (cellulose nanofibers) and CNCs (cellulose nanocrystals). There is evidence that oil-in-water emulsions can be stabilised by crystallinity in CNFs and CNCs (Tang et al., 2019). In recent years, nanocellulose has been extracted from different waste materials like banana peel, sunflower oil cake, peanut oil cake, sugarcane bagasse, etc. (Mandal and Chakrabarty, 2011; Harini et al., 2018; Kassab et al., 2019; Sumesh et al., 2020).

Pickering emulsions (PE), a type of emulsion stabilised by solid particles present at the oil-water interface, have gained attention because of their numerous applications in the food, pharmaceutical, and cosmetic industries. Scientific interest in PE stabilisation by oil-in-water (O/W) or water-in-oil (W/O) emulsions through formation of single layered colloidal particles is growing for possible implications in drug delivery (Erdagi et al., 2020). Due to the solid particles' irreversible adsorption to the oil-water interface and the surfactant molecules' rapid adsorption and desorption in response to thermal fluctuations, the system is extremely stable (Tang et al., 2019). PE were used for the encapsulation of bioactive compounds and essential oils like curcumin, carotenoids, marjoram essential oil, cumin seed oil, etc. (Ngwabebhoh et al., 2018; Almasi et al., 2020; Chutia and Mahanta, 2021; Foo et al., 2022). A controlled release of soluble and insoluble bioactive molecule from a PE is desirable. Because of their biocompatibility, lack of cytotoxicity, and ability to degrade, solid particles from natural sources have been utilised as stabilisers in PE systems over time (Erdagi et al., 2020). Inorganic or organic nanoparticles, such as silica, calcium carbonate, ferrous-ferric oxide, graphene, or microgel, titanium dioxide, lignin, starch, cellulose, and protein are among the solid particles

that are frequently utilised (Tang et al., 2019). Edible nanoemulsions have been employed in a range of supplementary formulations or in food and beverage fortified foods employing lipophilic bioactive substances such as oil-soluble vitamins, flavours, and minerals (Choi and McClements, 2020).

Curcumin, the main hydrophobic bioactive polyphenolic molecule present in the *Curcuma longa* plant has several medical uses (Ngwabebhoh et al., 2018). Curcumin has a variety of health advantages, including antimicrobial, antifungal, anti-inflammatory, antioxidant, anticancer, and antiviral properties (Choi and McClements, 2020). Unfortunately, curcumin is an unstable compound. At physiological pH, curcumin degrades to bicyclopentadione through autoxidation forming cleavage products such as vanillin, ferulic acid and bicyclopentadione (Kharat et al., 2017). When exposed to high temperatures, light, and an alkaline pH (>7), curcumin is quickly broken down. Additionally, due to its hydrophobic nature, it leaves the body quickly with little absorption in the digestive system (Aditya et al., 2015). Ngwabebhoh et al. (2018) prepared curcumin-enriched PE via oil-in-water approach stabilized by animated nanocellulose and observed a positive effect on emulsion stability at different pH levels. Pickering emulsions with encapsulated curcumin showed exceptional in vitro cytotoxicity for anticancer and antibacterial activities. A good antibacterial and antifungal impact was shown by antimicrobial activity of encapsulated curcumin against fungi, Gram-positive and Gram-negative bacteria with excellent inhibitory effectiveness. But in vitro release percentage of curcumin from the PE had reduced after 24 h of storage (Ngwabebhoh et al., 2018). Moreover, because curcumin is water insoluble and easily oxidised, it is challenging to use them in liquid food systems.

It is hypothesized that an optimal concentration of nanocellulose in the Pickering nanoemulsion may result in improved properties and stability of curcumin compared to conventional emulsions, due to the unique ability of nanocellulose to maintain emulsion integrity and prevent aggregation. In this study, we have formulated curcumin-enriched and nanocellulose-stabilized Pickering nanoemulsion via oil-in-water emulsion approach and fortified it in blended beverage of defatted coconut milk and pineapple juice to improve the encapsulation of curcumin in the novel beverage and to increase the bioaccessibility and stability of curcumin. While the nanocellulose from coconut milk waste residue has been explored, the stabilization of curcumin-enriched PE using this specific nanocellulose has been investigated for the first time. The main purpose was to determine the stability of the curcumin at different temperatures and pH levels, and to assess the effect of nanocellulose on PE. This approach of utilizing nanocellulose from coconut milk waste residue for stabilizing Pickering nanoemulsion and

incorporating them into blended beverages not only reduces environmental waste but also presents an economically and ecologically viable solution. Pickering nanoemulsion was prepared using high pressure homogenization of organic phase containing virgin coconut oil and Tween 80 with a hydrophilic aqueous phase containing nanocellulose, which encouraged the formation of nanocellulose-coated curcumin-enriched Pickering nanoemulsion via rapid dispersal of surfactant and oil into the aqueous phase containing the stabilizer. The curcumin-enriched Pickering nanoemulsion was characterised for particle size, microstructure, and emulsion stability.

5.2. Materials and methods

Coconuts were purchased from a local market in Tezpur. Non-ionic Tween 80 was used as a surfactant. Chemicals used for analysis were of Merck, TCI or SRL make. Standard curcumin (purity ≥98%) was obtained from Sigma-Aldrich.

5.2.1. Processing of coconut milk to obtain waste residue

Coconut milk waste residue was collected after extraction of coconut milk, dried in a tray dryer at 50 °C and ground into powder form and was coded as CMR.

5.2.2. Processing of coconut milk to obtain waste residue

5.2.2.1 Hemicellulose content in coconut milk waste residue

The hemicellulose content in CMR was determined using the method of Mansora et al. (2019). For this, 60 ml of acetone was added to 1 g coconut milk waste residue (CMR) and heated at 90 °C for 2 h. After 2 h of drying at 105-110 °C until constant weight, coconut milk waste residue coded as CMRB was obtained. Then, 150 ml of sodium hydroxide (0.5 mol/L) was added to 1 g of CMRB and heated for 3.5 h at 80 °C, after that the sample was washed with distilled water until it reached pH 7. The washed sample was dried at 105-110 °C until constant weight. This sample was coded as CMRC. Hemicellulose content was determined from Eq.5.1.

$$\text{Amount of hemicellulose (\%)} = \frac{\text{CMRB}-\text{CMRC}}{\text{CMRB}} \times 100 \qquad \text{(Eq.5.1)}$$

5.2.2.2 Lignin content in coconut milk waste residue

The lignin content in CMR was determined using the method of Mansora et al. (2019). For this, 1g of CMRB (from section 5.2.1.1) was added to 30 ml of 98% sulphuric acid. The sample was kept in sulphuric acid solution for 24 h and after that heated at 100 °C for 1 h. The mixture was washed with distilled water until pH 7 was obtained. After washing, the sample was dried

at 105-110 °C until constant weight was obtained. This sample was coded as CMRD. Final weight was recorded and lignin content was calculated using Eq.5.2.

$$\text{Amount of lignin (\%)} = \frac{\text{CMRB}-\text{CMRD}}{\text{CMRB}} \times 100 \quad \text{(Eq.5.2)}$$

5.2.2.3 Cellulose content in coconut milk waste residue

The cellulose content of CMR was determined using the method of Mansora et al. (2019). The total amount of coconut milk waste residue utilised in the experiment was 1 g. By calculating the difference between the initial weight of the sample with hemicellulose and lignin weight (from section 5.2.1.1 and 5.2.1.2), the cellulose content (CMRE) was determined.

1 g of coconut milk waste residue = (CMR - CMRB) + (CMRB - CMRC) + CMRD + CMRE (Eq. 5.3)

5.2.3. Preparation of nanocellulose

5.2.3.1. Acid hydrolysed nanocellulose

The powdered CMR was subjected to degumming with 1.5 L of hexane and ethanol (2:1) ratio (Alzate et al., 2019). To get rid of any residual solvent in the sample, the extracted lignocellulose powder was allowed to dry out at room temperature. The degummed residue was then alkali treated with 5% sodium hydroxide solution for 3 h, and the alkaline treated CMR was coded as ACMR. The alkaline treatment helped in the removal of pectin, wax, hemicellulose, and lignin, and enhanced the bonding ability of cellulose. After treatment, the alkaline layer was drained out and the sediment was washed using distilled water repeatedly to wash away any alkali and dried in an oven for 2 h at 70 °C (Sumesh et al., 2020). The ACMR sample was then treated with a mixture of nitric acid and acetic acid (65% v/v and 80% v/v, respectively), in a 1:10 ratio at 110 °C for 20 min with constant agitation. The amorphous solids were removed from solution after washing the obtained cellulose sample with ethanol and water before drying at 55 °C for 12 h (Alzate et al., 2019). This process gave the microcrystalline cellulose powder (MCP). Nanocellulose from MCP was prepared via acid hydrolysis methods as described by Ngwabebhoh et al. (2018) with modifications. In brief, 100 ml of different concentrations of sulfuric acid (38%, 40%, 42%) were added to 1g each of MCP, and the mixtures were magnetically agitated at 450 rpm for 120 min at 50 °C. To stop the hydrolysis process, the liquid was diluted ten times with distilled water. The suspension mixture was centrifuged at 4000 x g for 10 min, and then rinsed with distilled water for five times in a row to a pH of 7. The acquired sample was cleaned, centrifuged, and freeze dried

(Tang et al., 2014). The obtained suspensions treated with 38%, 40%, and 42% sulphuric acid were denoted as AC1, AC2, and AC3, respectively.

(a) (b) (c)

Fig 5.1: Preparation process of Nanocellulose (a) CMR (Cocont milk wate residue), (b) ACMR (alkaline treated coconut milk waste residue) and (c) ACU-10 (CMR hydrolysed with 42% acid and ultrasonicated for 10 min).

5.2.3.2. Ultrasound treated nanocellulose

The acid hydrolysed nanocellulose AC3 was further treated with ultrasound for 5 min and 10 min and coded as ACU-5 and ACU-10, respectively. MCP sample was ultrasonicated for 5 min (UL-5) and 10 min (UL-10) to determine the effect of ultrasonication on nanocellulose (without any acid hydrolysis) using a probe sonicator (U500, Takashi, Japan) at 80% vibration amplitude with pulse mode set for on/off for 3 s/3 s and 4.5 W/ml power.

5.2.4. Nanoemulsion preparation

The method of Gani et al. (2018) was used with some modification. Different concentrations of virgin coconut oil (VCO) (5-20%), Tween 80 (5-20%), and water were homogenized at 11,000 rpm for 5 min using a homogenizer (IKA, Model - T25, Digital Ultra Turrax). In accordance with the experimental design (Table 5.4), the well-mixed coarse emulsion was homogenised in a two-stage high-pressure homogenizer (GEA, Lab homogenizer Panda 2000, Italy) for five passes at 200–500 MPa to reduce the particle size to nanosize. Five numbers of passes were selected by trial-and-error method.

5.2.5. Optimization of nanoemulsion

Design-Expert Version 7.1.2 (Stat-Ease, Inc. MN), Response Surface Methodology (RSM) and face centred central composite design (FCCD) were used to optimize process conditions for the preparation of nanoemulsion. Three independent parameters: the amount of coconut oil (5-20%), concentration of Tween 80 (5-20%), and homogenizing pressure (200-500 bar) were

varied to see how they affected the emulsions' particle size and polydispersity index. ANOVA was performed to assess the importance of the model parameters under investigation. The significance level of $p \leq 0.05$ was used to determine its statistical significance.

The experimental variables, given in Table 5.1, were coded according to Eq. 5.4.

$$y_j = \frac{Y_j - Y_{j0}}{\Delta Y_j} \quad \text{(Eq.5.4)}$$

Where, Y_j and y_j indicated the actual and coded values of the "j" experimental variable, Y_{j0} was the actual value of the "j" experimental variable at the central point, and ΔY_j was the step change of the dimensionless value.

Table 5.1: Independent factors and their range set in face centred central composite design

Experimental Variables	Codes	Coded levels		
		-1	0	+1
Oil (%)	A	5	12.5	20
Surfactant (%)	B	5	12.5	20
Homogenizing Pressure (bar)	C	200	350	500

5.2.6. Pickering nanoemulsion preparation

The synthesis of Pickering nanoemulsion was done by following the method of Ngwabebhoh et al. (2018) with modification. Pickering nanoemulsion was developed using the optimised composition of VCO and Tween 80 using parameters given in Table (5.8). Curcumin (Cur) amount to be incorporated was determined after solubilising different concentrations in 100 ml of VCO. Accordingly, 0.2% w/v of curcumin in virgin coconut oil was taken for Pickering nanoemulsion development. The mixture was at first coarsely homogenised for 5 min at 11,000 rpm using a high-speed homogeniser (IKA, Model - T25, Digital Ultra Turrax), and thereafter homogenised under pressure (260 bar) conditions by combining the organic phase (oil and Tween 80) with an aqueous suspension (nanocellulose and water) having nanocellulose concentrations of 0.05, 0.1, 0.2, and 0.3 wt% for 5 passes. The synthesised Pickering nanoemulsions were coded as PN1, PN2, PN3 and PN4 for nanocellulose concentrations of 0.05, 0.1, 0.2, and 0.3 wt%, respectively and placed in glass vials to be stored at RT for further analysis.

5.2.7. Particle size measurement by dynamic light scattering (DLS)

Particle size of the different nanocellulose samples (AC1, AC2, AC3, ACU-5, ACU-10, UL-5, and UL-10) and Pickering nanoemulsion samples (PN1, PN2, PN3, and PN4) was measured by DLS (NanoPlus, Particulate systems, GA 30093-2901. U.S.A.) using the following conditions: 0.01 particle absorption coefficient, 1.59 particle refractive index, 1.33 water refractive index, 0.8872 cP viscosity, 25 °C temperature and general calculation model for irregular particles.

5.2.8. Characterisation of nanocellulose using FTIR analysis

The absorbance infrared spectra of the selected nanocellulose samples were captured using an FTIR spectrophotometer (Perkin Elmer, spectrum 100). The freeze-dried nanocellulose samples were measured at 400–4000cm^{-1} with a resolution of 2 cm^{-1}.

5.2.9. Characterisation of nanocellulose using XRD analysis

X-ray diffractometer (Model: D8 focus, Bruker) with Cu Kα radiation (λ = 0.154 nm) at 40 kV and 40 mA was used to analyse the crystallinity of the selected samples. The data were gathered at a scan range of 2θ = 5°- 40° and a scanning rate of 1°/min with resolution of 0.02º. Eq. 5.5 was used to determine crystallinity index.

$$\text{CI (\%)} = \frac{I002 - IAM}{I002} \times 100\% \qquad \text{(Eq.5.5)}$$

where I002 is the greatest intensity of the diffraction from 2Θ = 21° - 23° planes, representing both amorphous and crystalline material, IAM is the lowest height of peaks at 2Θ = 18º, indicating just amorphous material, and CI stands for the crystallinity index (Ishak et al., 2020).

5.2.10. Thermogravimetric analysis

A differential scanning calorimeter (NETZSCH, Model- DSC 214 POLYMA) was used to assess the thermal stability of selected nanocellulose samples using the method of Gué et al. (2016) with modification. For this, 3 mg of nanocellulose sample was weighed accurately into an aluminium pan and 7.5 µl distilled water was added using a micropipette. The pan was sealed and equilibrated for 4 h. At a temperature range of 25 °C – 400 °C, dynamic differential scanning calorimeter (DSC) scans were performed in a nitrogen atmosphere at a continuous heating rate of 2 °C/min. The thermograms were used to determine the crystallinity temperature and onset of melting temperature.

5.2.11. Morphology of nanocellulose

Field emission scanning electron microscopy (FESEM) was performed at a voltage up to 10 kV and magnifications of 100,000x and 30,000x. The FESEM (JEOL, model- JSM 7200 F) was used to examine the architecture of freeze dried nanocellulose and Pickering nanoemulsion samples. Sample was placed on the holder using double-sided cellophane tape and allowed to dry for 24 h. The samples were then exposed to iridium for 15 min.

5.2.12. Analysis of virgin coconut oil using gas chromatography-high resolution mass spectrometry (GC-HRMS)

The triglycerides and fatty acids in VCO were change into fatty acid methyl esters (FAMEs) by derivatization following boron trifluoride-methanol solution (BF_3-MeOH) method after alkaline hydrolysis, as outlined by Moigradean et al. (2013). Sample (20 mg) was added to 0.5 mol/L NaOH-methanol (2 ml), and the solution was heated for 7 min at 100 ℃. Afte cooling down the solution, 3 ml of 14% BF_3-MeOH reagent was added in sample solution and heated for 5 min at 100 ℃. After cooling, hexane and 7 ml of saturated NaCl were added, and the mixture was vigorously shaken. The obtained hexane layer (2 ml) was used for GC analysis using GC (Agilent, 7890, FID detector) and MS (Jeol, EI / CI source).

5.2.13. Solubility of curcumin

Using spectrophotometric analysis, the solubility of curcumin in olive oil and coconut was ascertained using the method of Joung et al. (2016). Curcumin was added in excess to the oil phase, which was then heated to 60 °C. After 10 min of stirring, the mixture was sonicated for 20 min using a bath sonicator (Riviera Glass Pvt. Ltd, India) at 230 volts and 50 Hz. The curcumin that was not dissolved in the oils was separated using a centrifuge (Eppendorf, model 5430 R, Germany) running at 1750 rpm for 10 min. Once the crystalline curcumin that had not dissolved was removed, the supernatant was diluted to the proper concentration and examined using a UV-Vis spectrophotometer (Cary 60 UV-Vis, Agilent). The amount of curcumin in each oil was tested at 415 nm. The curcumin solubility was calculated using a standard curve (0.05–1 g/100 ml) and was represented as g curcumin equivalent per 100 ml oil.

5.2.14. RP-HPLC analysis of curcumin-enriched Pickering nanoemulsion

The method based on Lu et al. (2018) was used to determine curcumin content in Pickering nanoemulsion (PN1, PN2, PN3, and PN4). RP-HPLC unit (ThermoFisher Ultimate 3000), C18 column (5µm, 120A, 4.6X 250 mm) and UV-Vis detector were used for the separation of curcumin using mobile phases of 0.1% formic acid in water (A) and acetonitrile (B) with the

following gradient conditions: 60% A and 40% B in the beginning decreased to 36% A at 7 min, maintained for 3 min, decreased to 10% A at 15 min, and returned to original ratio at 17 min with column temperature at 35 °C, flow rate at 1 ml/min at 425 nm wavelength. Curcumin content was identified by comparing retention time and absorption spectra and mass spectra of Pickering nanoemulsion peaks with reference standards. Six different concentrations (0.1, 0.5, 1, 5, 10, and 15 μg/ml) of curcumin standard were prepared in acetonitrile. The curcumin samples were then quantified from linear regression equation.

5.2.15. Stability test of curcumin-enriched Pickering nanoemulsion

Stability of curcumin-enriched Pickering nanoemulsion was determined using the method of Iqbal et al. (2020) and treated with whole spectrum of pH solutions (pH 2, 4, 6, and 8). The pH was adjusted using 1 N and 0.1 N hydrochloric acid and 1 N and 0.1N sodium hydroxide. The samples were then stored for 1 h at room temperature prior to analysis. Effect of heating conditions (63 °C for 30 min and 95 °C for 10 min) on curcumin content of Pickering nanoemulsions (PN1, PN2, PN3, and PN4) was studied. The stability of incorporated curcumin in Pickering nanoemulsion was determined using RP-HPLC analysis method of Lu et al. (2018) as mentioned in section 5.2.13.

5.2.16. Storage stability of curcumin-enriched Pickering nanoemulsion

The Pickering nanoemulsions were analysed for physical stability by percentage creaming index. For the test, 50 ml of the sample was placed in bottles; the bottles were tightly sealed and stored at 25 °C for 30 days. Nanoemulsion cracking was considered to have started when the oil and water layers had clearly separated and did not recombine (Pengon et al., 2018). Eq. 5.6 was used to compute the creaming index (CMI%).

$$\text{CMI\%} = \frac{CC}{CT} X 100 \qquad \text{(Eq. 5.6)}$$

Where, CT is the total height of the emulsion layer and CC is the total height of the cream layer.

5.2.17. Statistical analysis

Every component was analysed in triplicates, and results are given as the mean ± standard deviation of all separate studies. The data analysis was performed using IBM SPSS 20.0 software. The analysis of variance (ANOVA) and the Duncan's multiple range tests were performed to determine if there were significant differences between the values ($p < 0.05$).

5.3. Results and discussion

5.3.1 Cellulose, hemicellulose, and lignin content

After extraction of VCO from coconut milk, CMR (the waste residue) had 58.53±1.2% cellulose content, 23.59±2.1% hemicellulose, and 1.32±1.0% lignin. In comparison, Ishak et al. (2017) and Ng et al. (2010) reported that coconut dregs and coconut milk residue contained 36.1% - 72.7% cellulose, 2.0% - 12.6% hemicellulose, and 1.8% - 9.8% lignin.

5.3.2. Particle size and PDI analysis

The particle size distribution of the acid treated nanocellulose samples, namely, AC1, AC2 and AC3 that were subjected to acid concentration of 38%, 40%, and 42%, respectively for 120 min at 50 °C is presented in Table 5.2. The average particle size of AC1, AC2 and AC3 was 252.3 nm, 181.6 nm, and 176.0 nm, respectively. Particle size of the samples decreased with an increase in acid concentration. Rashid et al. (2021) also reported similar observation when the concentration of acid was increased from 40% to 78%. Tang et al. (2014) reported that concentration of sulfuric acid is a crucial factor influencing the extraction of nanocellulose during acid hydrolysis. However, the effect of acid concentration on particle size differed, as it was seen that the extent of reduction was severe at 42% concentration than at 38% and 40% concentration. While a sulfuric acid concentration that is too low could lead to unevenly dispersed or even aggregated fibres, a sulfuric acid concentration that is too high can significantly speed up the breakdown of cellulose into sugars. Theoretically, increasing sulphuric acid concentration for hydrolysis leads to a significant rise in SO_4^{-3} content. In the presence of SO_4^{-3} ions, nanocrystalline cellulose (NCC) carries a strong negative charge, resulting in optimal dispersion, particularly in water. The breakdown of cellulose chains and the aggregation of NCC are dependent upon the acid concentration used (Rashid et al., 2021). Many nanocellulose extraction processes require a high concentration of acid. However, using a lower acid concentration is more environment friendly as it reduces the amount of water needed in the washing step. Tang et al. (2014) and Harini et al. (2018) used 59 - 72% of sulfuric acid for hydrolysis, but in our sample 45-60% of acid concentration itself was severe enough to cause serious degradation of the cellulose sample CMR. It implied that the right concentration of sulfuric acid differed from sample to sample. Phanthong et al. (2015) reported the use of 47% sulfuric acid for nanocellulose extraction along with mechanical process (ball-milling).

PDI value of AC1, AC2, and AC3 was 1.00, 1.00 and 0.2, respectively. Typically, PDI below 0.4 describes the unimodal peak and is said to be monodisperse and for PDI more than 0.4,

bimodal and trimodal peaks are observed (Keshavamurthysetty and Patel, 2023). The controlled acid hydrolysis can selectively break down the amorphous zones and yield crystalline nanocellulose particles that are of small size, as seen for AC3. The resulting particle size is, therefore, largely influenced by the cellulose source and its proportion of amorphous content. Additionally, the reaction rate is influenced by the concentration of acid, time, and temperature of hydrolysis reaction (Wulandari et al., 2016). Acid concentration up to 40% yielded PDI value of 1.00 (AC1 and AC2). There was a steep decrease in PDI when acid concentration was increased to 42%, as noticed for AC3 (PDI 0.178), indicating the significance of acid concentration used. As AC3 exhibited small particle size and lowest PDI, it was taken for ultrasonic treatment.

Particle size of 133.4 nm and 149.9 nm, and PDI value 0.7 and 0.6 was measured for UL-5 and UL-10, respectively that were produced by the ultrasonication approach. Ultrasonication treatment alone was observed to be ineffective in breaking the strong hydrogen bonds of native fibres, therefore, the PDI value of UL-5 and UL-10 was higher than 0.4, which shows that the particles were unstable and uneven in size.

Table 5.2: Particle size and polydispersity index of nanocellulose samples

Samples	Average particle size (nm)	Polydispersity index
AC1	252.3	1.0
AC2	181.6	1.0
AC3	176.0	0.2
UL-5	133.4	0.7
UL-10	149.9	0.6
ACU-5	59.1	1.0
ACU-10	99.6	0.2

ACU-5 (CMR hydrolysed with 42% acid and ultrasonicated for 5 min); ACU-10 (CMR hydrolysed with 42% acid and ultrasonicated for 10 min); AC1 (CMR hydrolysed with 38% acid); AC2 (CMR hydrolysed with 40% acid); AC3 (CMR hydrolysed with 42% acid); UL-5 (microcrystalline cellulose powder (MCP) sample was ultrasonicated for 5 min); and UL-10 (MCP sample was ultrasonicated for 10 min).

The acid hydrolysed nanocellulose, AC3 that was subjected to ultrasonication treatment for 5 and 10 min to obtain ACU-5 and ACU-10, respectively showed a particle size of 59.17 nm and 99.65 nm, and PDI value 1.00 and 0.2, respectively. The ACU-10 recorded lowest PDI as

compared to ACU-5, due to the combined effect of both chemical and mechanical methods that helped in better removal of amorphous regions from AC3. The emission of heat due to cavitation effect leads to bond breakage and further disintegration of the nanocellulose obtained after acid hydrolysis (Tang et al., 2014). Danaei et al. (2018) reported that PDI value of 1.0 gives an indication that the sample has diverse particle sizes. The authors opined that for polymer-based nanoparticles, the PDI value of <0.2 or lower is typically considered satisfactory, whereas in drug delivery system, especially when using lipid-based carriers the PDI of 0.3 or lower is viewed as desirable. Liu et al. (2023) reported that the walnut protein isolate nanoparticle with average particle size of 108 nm and a PDI value of 0.40 showed good solubility, uniform solution, and no precipitation as compared to walnut protein isolate with PDI value of 0.56. Similar observation was observed for sample ACU-10. Thus, combination of acid hydrolysis and ultrasonication treatment yielded nanocellulose with small aspect ratio as compared to only ultrasonication. ACU-10 can be used for the stabilization of Pickering emulsion. It has been reported that a smaller aspect ratio allows for higher nanocellulose addition to a matrix (Cao et al., 2019).

5.3.3. Characterisation of nanocellulose using FTIR analysis

As shown in Fig. 5.2, there are mainly twelve peaks in all the treated samples that are marked as A, B, C, D, E, F, G, H, I, J, K and L with positions at 3400 $cm^{-1,}$ 2927 cm^{-1}, 2890 cm^{-1}, 1743 cm^{-1}, 1640 cm^{-1}, 1424 cm^{-1}, 1378 cm^{-1}, 1369 cm^{-1}, 1105 cm^{-1}, 1056 cm^{-1}, 890 cm^{-1}, and 725 cm^{-1}. AC3, UL-10, and ACU-10 exhibited the same cellulose I characteristic absorption peaks, which are attributed to OH groups, and CH_2 groups. These peaks were not observed in CMR. The absorption peak observed at 3400 cm^{-1}, 2900 cm^{-1}, 1430 cm^{-1}, 1370 cm^{-1}, and 890 cm^{-1} are for intermolecular hydrogen attached at C-H, C-O bonds, and C_6 group in the polysaccharide aromatic ring, and β-glycosidic linkages between glucose and cellulose (Yang et al., 2017). There were two main absorbance areas found in all samples. The first one at short wavelengths, roughly between 700 and 1,800 cm^{-1}, and the second one at longer wavelengths, roughly between 2,700 and 3,500 cm^{-1}. Nonetheless, distinct absorption peaks for each distinct component could be found.

The peak at D which is observed in all four samples except ACU-10 corresponds to the presence of small amounts of hemicellulose because of the higher C=O linkage at 1765-1715 cm^{-1}, which is removed completely in ACU-10 sample due to the combination of both acid and ultrasound treatment (Morán et al., 2008; Wulandari et al., 2016). Absorption peak marked as C that denotes C-H stretch in CMR is not observed in nanocellulose samples. Mandal and Chakrabarty (2011) also reported C-H stretching vibration around 2894 cm^{-1}. Morán et al.

(2008) observed OH bond at 1640 cm^{-1} for adsorbed water, even though the FTIR samples were developed following careful drying process, suggesting that the water adsorbed in the cellulose molecules is very difficult to extract due to the cellulose-water interaction. The OH bond at E was observed in AC3, UL-10 and ACU-10 but not in CMR. Mariño et al. (2015) attributed the band around 1375 cm^{-1} to C-H bending in cellulose with high crystallinity index. The nanocellulose samples AC3, UL-5 and ACU-10 presented the characteristic C-H band at 1378 cm^{-1} which was not present in CMR. The CH_2 symmetric bending at 1424 cm^{-1}, the CH_2 wagging bending at 1318 cm^{-1} and the C-O-C motions of the β-glycosidic linkages at 1102–1105 cm^{-1}, 1054–1056 cm^{-1} and 725 cm^{-1} can be explained by the CH_2 rocking and –HC=CH– (*cis*) bending mode of molecular vibrations.

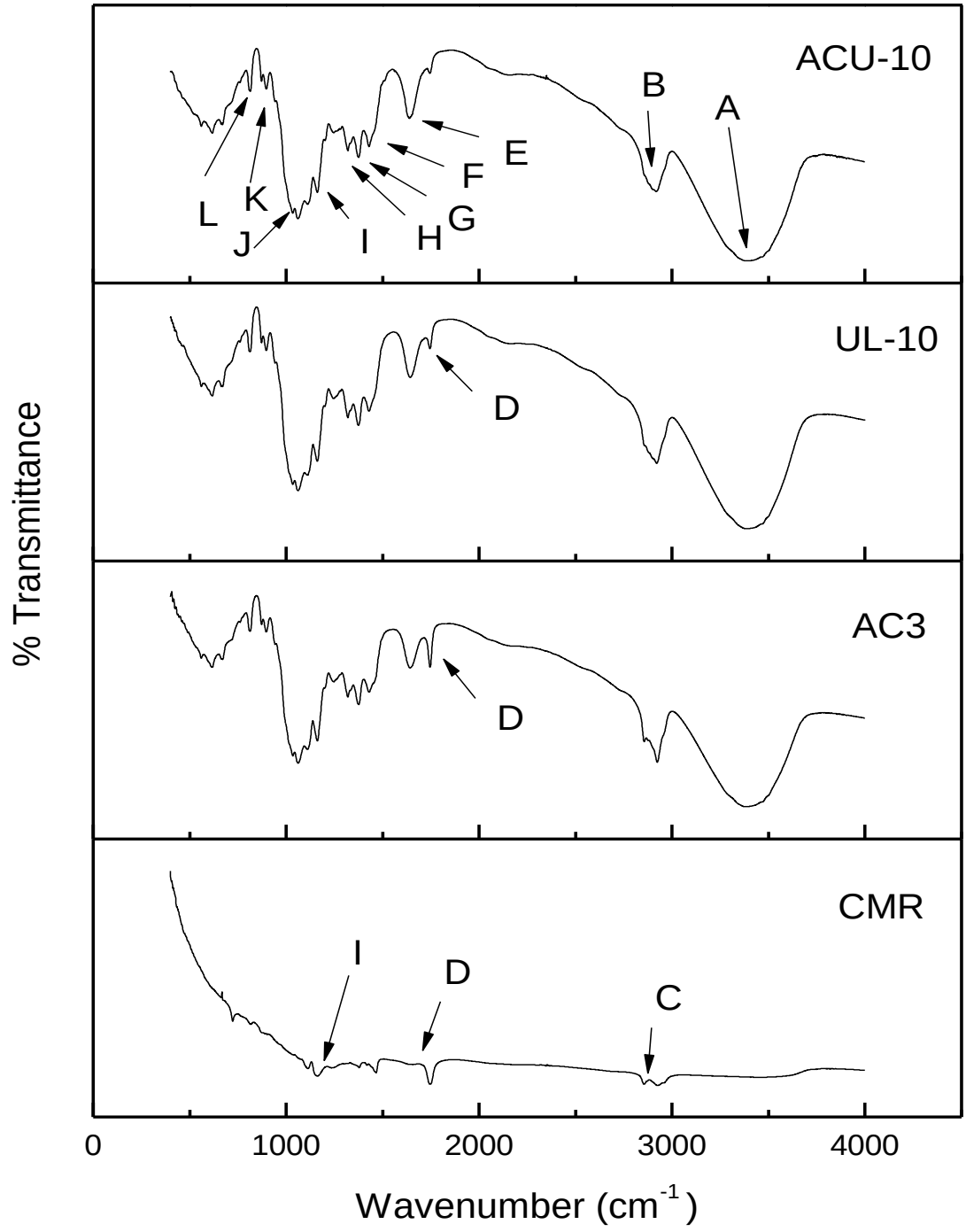

Fig 5.2: FTIR spectra of CMR (coconut milk waste residue), AC3 (CMR hydrolysed with 42% acid), UL-10 (MCP sample was ultrasonicated for 10 min), and ACU-10 (CMR hydrolysed with 42% acid and ultrasonicated for 10 min).

5.3.4. Crystallinity index of nanocellulose

X-Ray diffractograms of CMR and nanocellulose samples are presented in Fig. 5.3. All of the nanocellulose samples had higher peak intensities than the Control sample, indicating that the nanocellulose samples are more crystalline. The crystallinity index of CMR, AC3, ACU-10, and UL-10 was 20.0%, 30.4%, 35.5%, and 29.4%, respectively. Thus, the crystallinity of ACU-

10 increased the most. The amorphous area or the defective crystalline portions only got destroyed after the acid hydrolysis, which resulted in the evident increase of crystallinity of AC3 and ACU-10. This is because the crystalline components are more resistant to chemical treatments. The crystalline structure of nanocellulose is formed because of inter and intra hydrogen bonding, along with the van der Waals interaction between the polymeric chains. However, during the hydrolysis of microcrystalline cellulose, the disconnection of inter-linkages leads to a reorganization of the polymeric linkages. Due to the hydrolysis reaction of acid in AC3 and ACU-10, the H^+ ions are able to penetrate more in amorphous regions of cellulose and allow the hydrolytic cleavage of glycosidic bonds resulting in individual crystallinity. Moreover, microcrystalline cellulose hydrolysed with acid eliminates the amorphous regions of microfibrils, which promotes the formation of nanocrystalline cellulose with consequent reduction of the particle diameter from micron to nano level (Rashid et al., 2021). Furthermore, acid hydrolysis combined with ultrasonic treatment further improve the crystallinity as obtained in ACU-10 sample. The ACU-10 with small particle size and lowest PDI as compared to other nanocellulose samples (AC3, UL-10) showed better crystallinity due to the combined effect of both chemical and mechanical methods that helped in better removal of amorphous regions from CMR than AC3. The emission of heat due to cavitation effect leads to bond breakage and further disintegration of the nanocellulose is seen after acid hydrolysis (Tang et al., 2014). Thus, ultrasonication further improves the crystalline behavior of nanocellulose. Results indicated that ACU-10 with lowest PDI (0.166) displayed the maximum crystallinity index of 35.5%. Nanocellulose with higher crystallinity usually has better mechanical properties. Crystallinity was higher in nanocellulose subjected to acid hydrolysis in comparison to only ultrasonication. Nanocellulose obtained by mechanical treatment has both amorphous and crystalline regions, whereas the amorphous regions get easily hydrolysed during acid hydrolysis while the crystalline regions show a higher resistance to acid attack. Similar observations were made by Yang et al. (2017). Due to this difference in treatment behavior, the UL-10 sample had lower crystallinity as compared to AC3 and ACU-10. Further, ACU-10 that had the highest crystallinity also registered lower particle size and PDI among all the nanocellulosic samples, which increased its stability**.** Harini et al. (2018) estimated crystallinity index of 28.6% and 75.8%, respectively in banana bract micro and nano cellulose fibers.

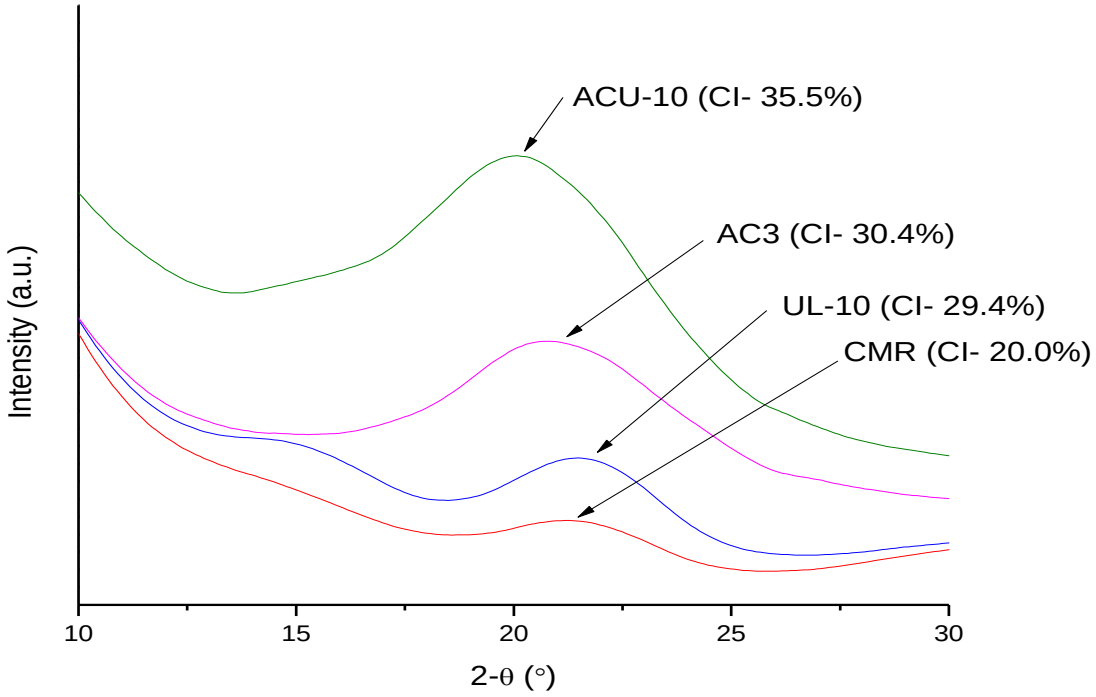

Fig 5.3: X-ray diffractograms of CMR (coconut milk waste residue), AC3 (CMR hydrolysed with 42% acid), UL-10 (MCP sample was ultrasonicated for 10 min), and ACU-10 (CMR hydrolysed with 42% acid and ultrasonicated for 10 min).

5.3.5. Thermogravimetric analysis

Fig. 5.4 displays the DSC thermograms of nanocellulose samples and CMR. All the thermograms showed clear endothermic changes. The characteristics of endotherms varied from one another and were extremely specific to the material's composition. Initial peak of DSC that is observed at lower temperature (<100°C) corresponds to evaporation of water (Tang et al., 2014). Generally, the second endothermic peak of nanocellulose indicates the course of fusion or melting, which gives an idea of the nature of decomposition of nanocellulose. In AC3 and ACU-10 samples, the melting peaks of nanocellulose were observed at 240 °C and 247.9 °C, respectively. AC3 and ACU-10 showed wider endothermic peak corresponding to the fusion of its crystalline part. Nanocellulose obtained from ultrasound treatment method, i.e., UL-10 did not show a sharp fusion peak but just a small curve at 314 °C. The melting peaks of the crystalline nanocellulose were observed in the temperature range of 230 °C - 250 °C by Maiti et al. (2013). The higher onset of decomposition temperature and endotherm width plays a vital role in determining the crystallinity of nanocellulose sample (Ishak et al., 2020). Thus, the nanocellulose AC3 and ACU-10 displayed the DSC patterns in the investigated temperature range that was not observed in CMR sample, because CMR contained different amounts of

non-cellulosic components including hemicellulose, lignin, pectin, etc. Mandal and Chakrabarty (2011) reported a higher onset of crystalline melting temperature of sugarcane waste nanocellulose extracted by acid hydrolysis, but within a narrow endotherm width in temperature range of 253–290 °C. The accessible hydroxyl groups as present in alkali treated (to remove pectin, wax, hemicellulose and lignin) sample are sulfated during acid hydrolysis and the comparatively bulky sulphate groups bring about rearrangement of crystal compactness. The amorphous areas also experience similar sulfation. The commencement of fusion in nanocellulose during heating occurs earlier than in cellulose because of the shift in orientation and the concurrent decrease in molecular weight or degree of polymerization. Acid hydrolysis leads to a breakdown in length of molecular chain possibly by hydrolyzing the pyranosyl linkage and forming small length of crystallites. This caused higher crystallinity in AC3 and ACU-10 samples. Extraction of nanocellulose from AC3 by acid hydrolysis and ACU-10 by a combination of acid hydrolysis and ultrasonication treatments may have removed the amorphous region and shifted the crystalline peak to 240 °C and 247.9 °C, respectively. Ultrasonic treatment facilitates the interaction between single fiber and microbubbles produced by acoustic cavitations (Tang et al., 2014), which further disintegrates the amorphous regions left after acid hydrolysis that resulted in enhanced crystallinity. The increase in the position of the peak can be related to the decrease in the amount of amorphous region in the cellulose crystallite length (Morán et al., 2008), as seen in XRD graph (Fig. 5.3), which shows that the crystallinity of ACU-10, AC3 and UL-10 increased as compared to CMR, and ACU-10 showed somewhat greater crystallinity as compared to AC3 and UL-10; these results are also supported by the melting peaks of DSC. On the other hand, UL-10 did not show wide endotherm peak during melting and its crystallinity was also lower, as observed in XRD analysis. The shift of the peak in UL-10 was more likely due to the wider molecular weight and size distribution of cellulose crystals (Morán et al., 2008). Numerous research studies have determined that cellulosic materials with high crystallinity generally exhibit enhanced thermal stability (Santmartí and Lee, 2018).

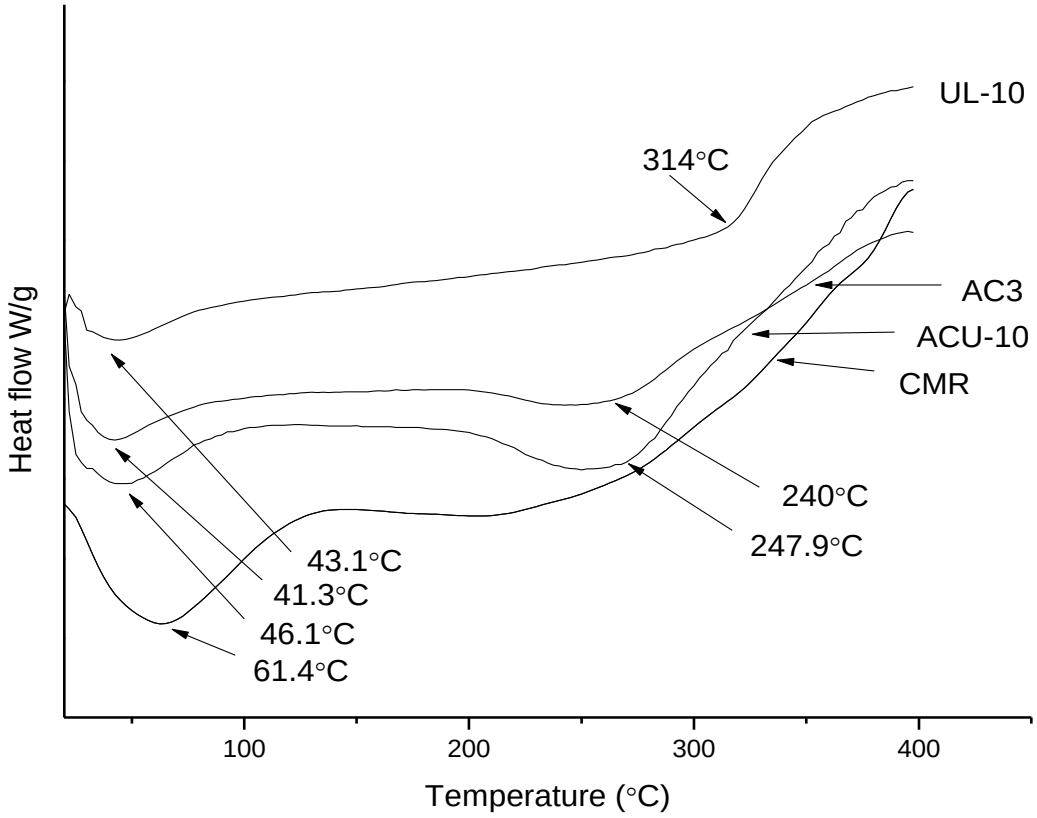

Fig 5.4: Differential scanning calorimetry graphs of CMR (coconut milk waste residue), AC3 (CMR hydrolysed with 42% acid), UL-10 (MCP sample was ultrasonicated for 10 min), and ACU-10 (CMR hydrolysed with 42% acid and ultrasonicated for 10 min).

5.3.6. Morphology of nanocellulose

Fig. 5.5(a-g) presents the FE-SEM micrographs of nanocellulose samples. The structure of dense non cellulosic components such as pectin, lignin, and hemicellulose were intact in CMR. Fig. 5.5(a) clearly demonstrates that CMR sample contained numerous non-fibrous components like the naturally present wax and oil that were spread over the surface prior to pulping and bleaching. After sodium hydroxide treatment of CMR (Fig. 5.5b), holocellulose was produced by the gradual removal of lignin. Fig. 5.5(c and d) showed that lignin and other impurities were removed through chemical purification of AC3 but some amorphous regions are still intact. The refinement of the fibrillar structure together with additional reduction in its width and sporadic breakdown of the fibrillar structure in its axial direction were seen in Fig. 5.5(c and d). The intact nanocellulose structure of UL-10 may have resulted from the presence of certain non-cellulosic amorphous areas as seen in Fig. 5.5 (e and f). Yang et al. (2017) reported that the strong hydrogen bonds in native fibers cannot be effectively broken by ultrasonication treatment, leaving behind most of the amorphous areas and a widespread dispersion of nanocellulosic matter as such. Fig. 5.5(g and h) showed that ACU-10 sample has

resulted in the separation of nanofibrils from fiber bundles, leading to a uniform distribution of cellulose nanofibers, as was also observed by Asem et al. (2023). The fiber's length was up to several micrometres and the fiber length could not be precisely measured due to the random entanglement and non-visible ends. This suggested the possibility of a high ratio between the extracted fiber's nanoscale diameter and microscale length.

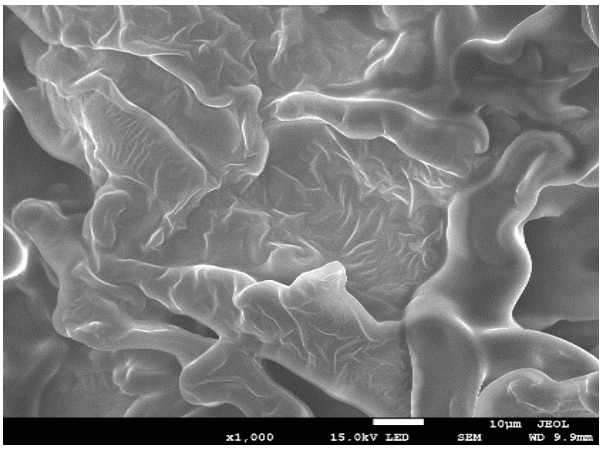

(a)

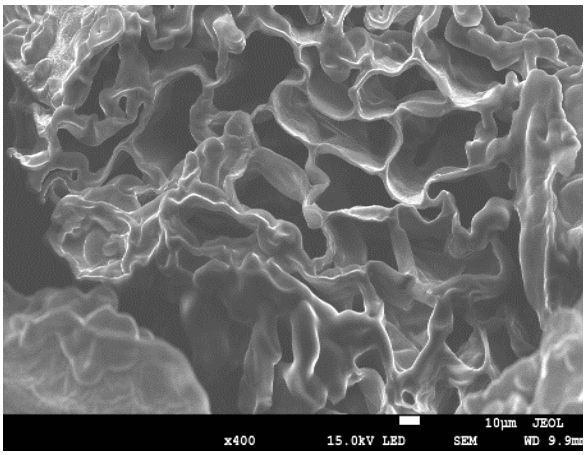

(b)

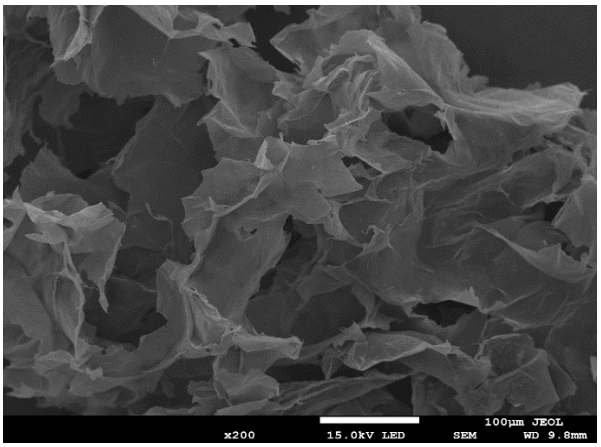

(c)

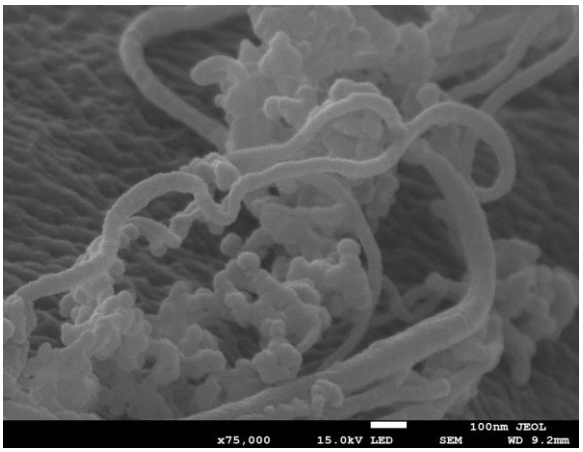

(d)

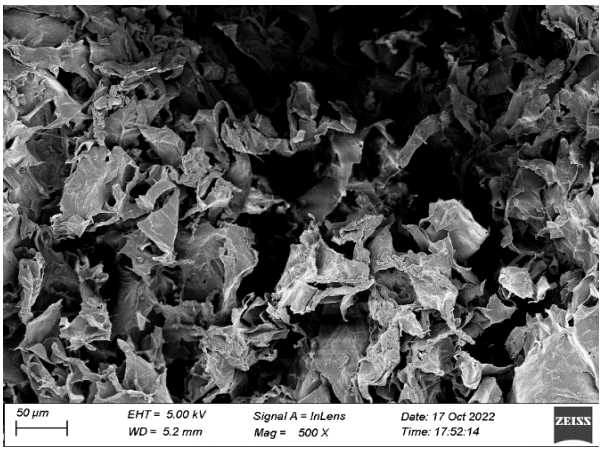

(e)

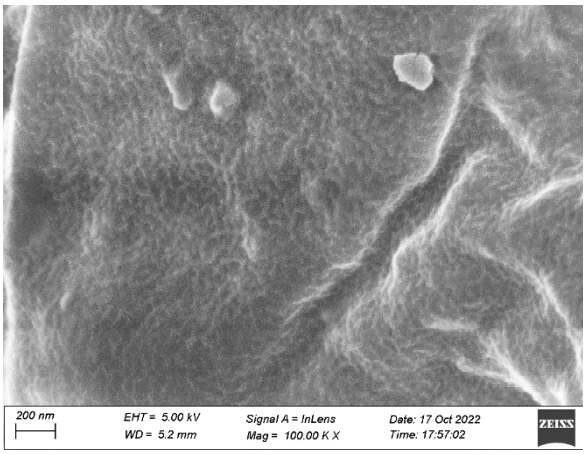

(f)

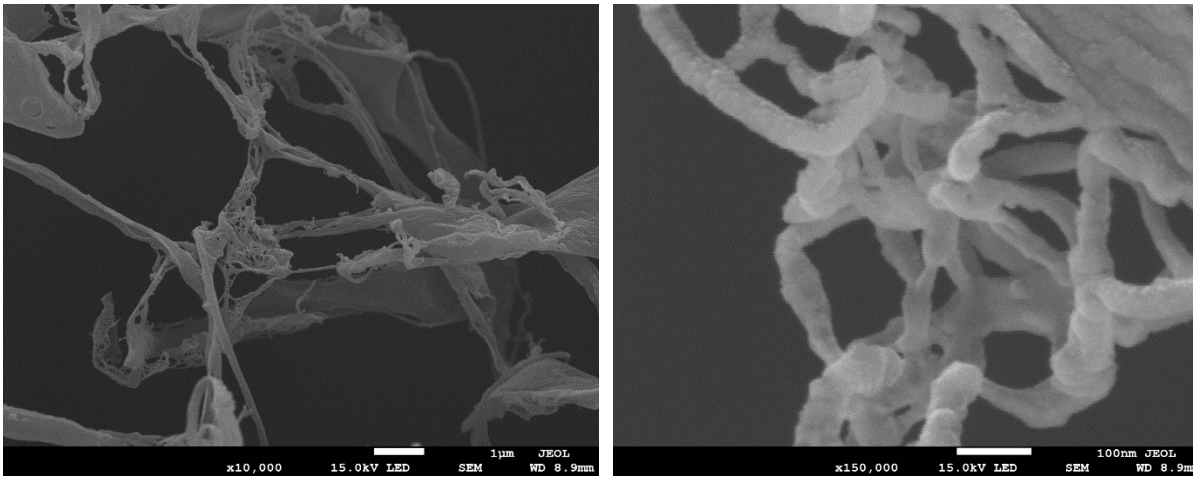

(g) (h)

Fig 5.5: FE-SEM micrographs in micrometre range and nanometre range; (a) CMR (coconut milk waste residue) (b) ACMR (Alkaline treated coconut milk waste residue), (c & d) AC3 (42% sulphuric acid treated CMR), (e & f) UL-10 (MCP sample was ultrasonicated for 10 min), and (g & h) ACU-10 (AC3 was further treated with ultrasound treatment for 10 min).

5.3.7. Composition of virgin coconut oil

GC-HRMS analysis of VCO is shown in Table 5.3. The fatty acid composition revealed that the oil is rich in medium chain fatty acids and contains nearly 49.3% lauric acid, 0.6% caproic acid, 7.47% caprylic acid, 5.9% capric acid, 18.5% myristic acid, 2.8% palmitic acid, and 6.1% stearic acid (Table 5.3, Fig 5.6). These fatty acids are known to have antibacterial, antifungal and antiviral properties (Nasir et al., 2018). Raghavendra and Raghavarao (2010) reported 47.4% lauric acid content, 0.7% caprylic acid, 3.7% capric acid, 23.5% myristic acid, 11.1% palmitic acid, and 3.9% stearic acid in commercial coconut oil, which is lower than the VCO extracted in this study (Table 5.3).

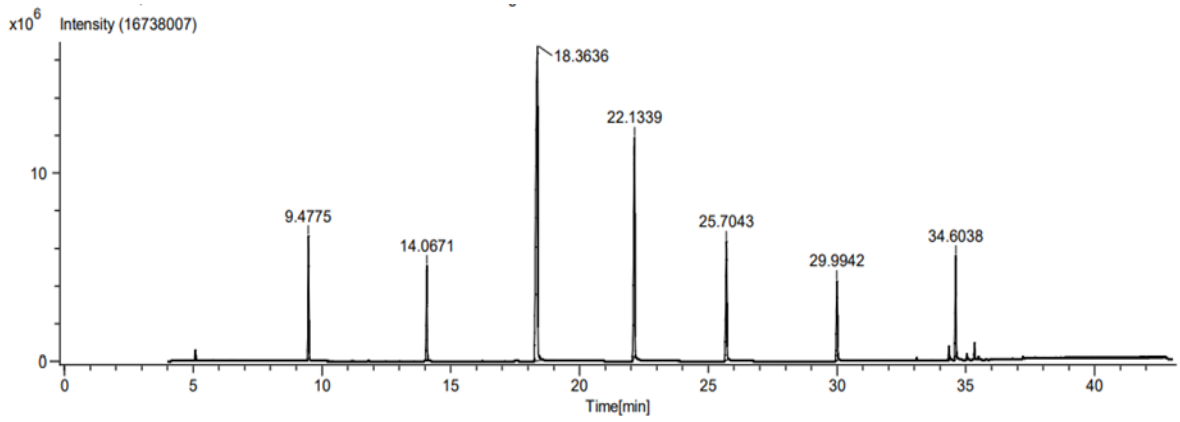

Fig 5.6: GC-MS chromatogram showing peaks of fatty acids present in virgin coconut oil.

Table 5.3. Fatty acids composition of virgin coconut oil

S. No	Peak time (min)	Fatty acids	Fatty acid content (%)
1	5.0811	Caproic acid methyl ester	0.6
2	9.4775	Caprylic acid methyl ester	7.9
3	14.0671	Capric acid methyl ester	5.9
4	18.3636	Lauric acid methyl ester	49.3
5	22.1339	Myristic acid methyl ester	18.5
6	25.7043	Palmitic acid methyl ester	2.8
7	29.9942	Stearic acid	6.1
8	33.0917	Arachidic acid methyl easter	0.1
9	34.6038	Hexadeconoic acid 10-hydroxy-methyl ester	0.9
10	35.0434	Octadeconoic acid 9,10-dihydroxy-methyl ester	6.9
11	35.3365	Octadeconoic acid 9,10-dichloro-methyl ester	0.3

5.3.8. Solubility of curcumin

VCO was extracted from coconut milk using chilling technique to separate the fat from coconut milk. Fat content in coconut milk was 21.2±0.03% and after its removal, the fat content was 0.3±0.02%. The removed fat was used as a VCO for development of nanoemulsion to incorporate curcumin. The solubility of curcumin in VCO was measured to determine the appropriate amount to be added for nanoemulsion development. (Joung et al. (2016) reported that the solubility of curcumin was high in MCT oil. VCO contains mixture of medium chain triglycerides and long chain triglycerides. The solubility of curcumin in VCO and olive oil was 0.20±0.01 g/100 ml and 0.19±0.02 g/100 ml (Table 5.4), respectively. (Joung et al. (2016) reported that the solubility of curcumin in normal coconut oil and olive oil was 0.1 mg/ml and 0.08 mg/ml, respectively. Kanchanathawornviboon et al. (2021) observed that the solubility of curcumin was high in virgin coconut oil i.e. 0.06% as compared to 0.04% in coconut oil, indicating higher solubility in VCO than normal coconut oil. This might be due to the higher concentration of MCT present in VCO as compared to coconut oil (section 5.3.7).

Table 5.4. Solubility of curcumin in oils

Samples	Curcumin solubility (g/100 ml)
Virgin coconut oil	0.20±0.01[a]
Olive oil	0.19 ±0.02[a]

5.3.9. Optimization of nanoemulsion

5.3.9.1. Effect of oil content, surfactant content, and homogenization pressure on particle size and PDI value of nanoemulsion

For preparation of a stable nanoemulsion, the concentration of the oil phase is very important. Keeping this in mind, the impact of the oil phase concentration on the droplet size of nanoemulsion produced during high-energy emulsification was assessed, as shown in the response surface plots presented in Fig 5.7. (a, b, d and e)**.** The nanoemulsion size was found to slightly decrease in particle size and PDI as the oil content was increased up to 7%, thereafter increase in the size and PDI values were observed with a further increase in oil concentration. From the ANOVA table, the overall effect of oil content was found to be significant for size ($p< 0.05$) and non-significant for PDI value ($p>0.05$) (Table 5.6 and 5.7).

Generally, the physicochemical properties of organic phase containing oil and stabilizers affect the size of the droplets size. The viscosity of the oil may have an impact on the interfacial tension and the transit rate at which non-ionic surfactant molecules move from the organic phase to the aqueous phase (Ngwabebhoh et al., 2018). The oil phase concentration was thus changed by utilizing an FCCD design model to mix distinct mass ratios of VCO and Tween 80 at varying concentrations. The particle size and PDI value decreased as homogenization pressure increased from 200 bar to approximately 260 bar (Fig. 5.7. a, c, d and f) followed by an increase in size and PDI with further increase in pressure, while other parameters remained constant. The size of droplet and PDI value was seen to gradually increase with an increase in stabilizer concentration from 5 to 20% as shown in the response curves (Fig. 5.7. b, c, e and f), so our desired minimum size was obtained near the lowest surfactant content. For both particle size and PDI value, the effect of stabilizer was found to be significant.

Homogenization pressures are normally used between 200 and 500 bar in the industry (Wang et al., 2008). So, in this study, pressure was chosen in the industrial range only. The effects of pressure on responses, particles size, and PDI was found to be significant ($p<0.05$) (Table 5.6 and 5.7). Similar trend was observed by Chutia and Mahanta (2021). Particle size, viscosity,

and environmental parameters like temperature and shear force can all have an impact on emulsion stability. As they are more abundant at a given phase ratio and more prone to Brownian motion, which increases the likelihood of collision, smaller particles generally have a weaker inclination to cream but a larger tendency to aggregate (Yuan et al., 2008).

As shown in Fig 5.7 a, b, and d, the nanoemulsion size was found to slightly decrease in particle size and PDI with an increase in oil content up to 7%, thereafter increase in the size and PDI values were observed with a further increase in oil concentration. Thus, increase in oil content reduces the overall size of emulsion droplets up to a certain point. However, once this point is reached, no further disintegration happens, and the size increases, most likely as a result of the excessive oil accumulating as a thick layer on the surface (Ding and Kan, 2017). It was found that the total effect of oil content on the particle size reduction process was significant ($p<0.001$), as shown in Table 5.7**.**

The effect of pressure on particles size and PDI of emulsion was significant with $p=0.0001<0.05$ (Table 5.6) and $p=0.004<0.05$ (Table 5.7), respectively. The particle size and PDI value decreased as pressure was increased (Fig 5.7 a, c, and f). The combination of shearing, grinding, and cavitation causes the disintegration of emulsion particles and droplets during HPH treatment (Ding and Kan, 2017; Romanski et al., 2011). Higher pressure results in increased melting, which raises the temperature and leads to agglomeration (Wang et al., 2008; Guo et al., 2019). Fig 5.7 a, c, and f shows that the effect of high pressure on size reduction was positive.

The models (Table 5.6 and Table 5.7) were well-fitting ($p\leq0.05$), as evidenced by the strong correlation between the experimental data and the predicted values determined by the model equation. Particle size and PDI value had R^2 values of 0.91 and 0.75 respectively, indicating a strong correlation between the input and response variables. Lack-of-fit was found to be non-significant for both response parameters, and the model was highly significant for particle size ($p= <0.0001$) and PDI ($p= 0.0114$), respectively. This validated the models, meaning that they could effectively explain the experimental data.

Based on maximum desirability level of 0.93, optimized conditions that were obtained were: 6.95% oil, 5% stabilizer (Tween 80) and 256.50 bar pressure (Table 5.8). Under the conditions applicable in the laboratory (6.95% oil, 5% stabilizer (Tween 80) and 300 bar pressure), the predicted particle size and PDI values were 191.807 nm and 0.189 respectively, whereas the optimal experimental values were 198.24 nm and 0.21, respectively. Pengon et al. (2018) reported that addition of polyethylene glycol hydrogenated castor oil (PHC) at 5%

concentration was suitable for the preparation of coconut oil nanoemulsion resulting in a droplet size of 0.162 µm. Furthermore, droplet size of nanoemulsion decreased from 33 µm to 200 nm with an increase in the amount of PHC from 1% to 10% w/w. Homogenization can significantly affect the property of emulsion, as the shear force and turbulence produced during homogenization are pressure dependent and affects the particle size of nanoemulsion. Yuan et al. (2008) found particle size of nanoemulsion to decrease with an increase in the homogenization pressure from 60 to140 MPa.

5.3.9.2. Modelling and validation

Design-Expert (Design-Expert Version 7.1.2 software, Stat-Ease) was used to analyse statistically all the experimental data, that were determined in accordance with FCCD design. The quadratic polynomial equations (Eq. 5.7 and 5.8) fitted with all the experimental data explained the effect of homogenization pressure, stabilizer, and oil on particle size and PDI values of the nanoemulsion.

$$\text{Particle size} = + 290.23+89.15*A + 60.51*B - 98.89*C + 32.59*A*B - 44.21*A*C - 22.31*B*C + 34.60*A^2 \quad \text{(Eq. 5.7)}$$

$$\text{PDI value} = + 0.31+0.075*A +0.051*B - 0.086*C - 0.059*A*C - 0.015*B*C - 0.046*B^2 + 0.041*C^2 \quad \text{(Eq. 5.8)}$$

R^2 values obtained were 0.91 and 0.75 for particle size and PDI of nanoemulsion, respectively (Table 5.6 and 5.7) using different processing parameters such as homogenization pressure, stabilizer, and oil concentration. The quadratic model having higher R^2 indicates a good correlation between responses and input parameters. A CV% score of less than 10% indicated well fit of model for data. The models were validated (Table 5.8) by non-significant lack of fit for responses. The models high level of significance with $p=<0.0001$ for particle size and $p=0.0114$ for PDI value, explained the high efficiency of experimental data.

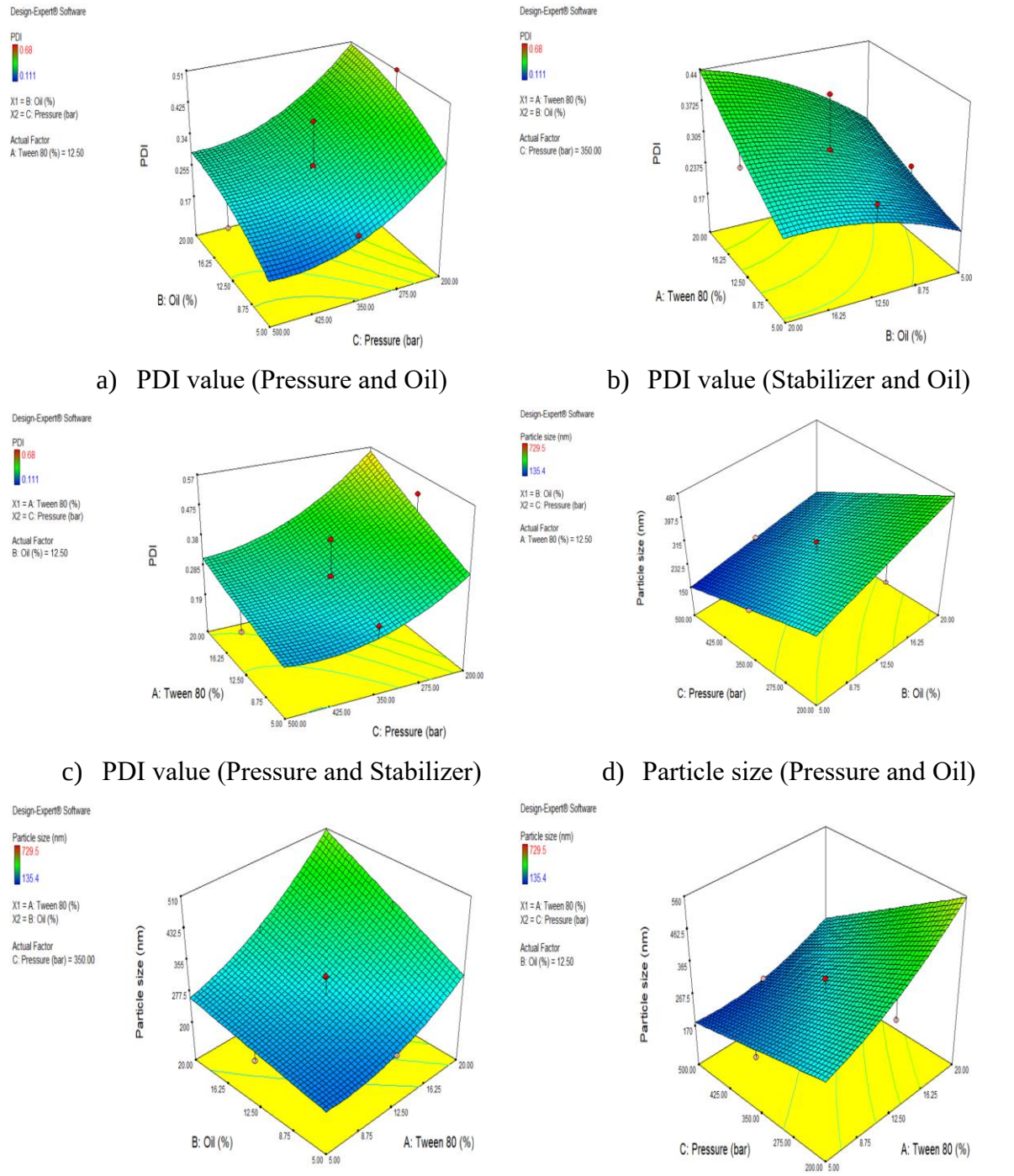

a) PDI value (Pressure and Oil)

b) PDI value (Stabilizer and Oil)

c) PDI value (Pressure and Stabilizer)

d) Particle size (Pressure and Oil)

e) Particle size (Stabilizer and Oil)

f) Particle size (Pressure and Stabilizer)

Fig. 5.7. Response surface 3D plots showing effect of pressure, oil, and stabilizer on: (a) PDI value (Pressure and Oil), (b) PDI value (Stabilizer and Oil), (c) PDI value (Pressure and Stabilizer), (d) Particle size (Pressure and Oil), (e) Particle size (Stabilizer and Oil), (f) Particle size (Pressure and Stabilizer).

Table 5.5. Experimental design matrix of the effect of stabilizer, oil, and high-pressure homogenization pressure on particle size and PDI value

Experimental run	Independent variables			Responses	
	Factor 1 Tween 80 (%)	Factor 2 VCO (%)	Factor 3 Pressure (bar)	Response 1 Particle size (nm)	Response 2 PDI value
1	5	5	200	285.0	0.21
2	20	5	200	422.8	0.37
3	12.5	12.5	200	327.0	0.52
4	5	20	200	322.5	0.22
5	20	20	200	729.5	0.65
6	12.5	5	350	226.8	0.23
7	5	12.5	350	213.0	0.27
8	12.5	12.5	350	317.5	0.30
9	12.5	12.5	350	248.5	0.30
10	12.5	12.5	350	317.5	0.22
11	12.5	12.5	350	317.0	0.30
12	12.5	12.5	350	317.5	0.42
13	12.5	12.5	350	317.5	0.3
14	20	12.5	350	368.6	0.31
15	12.5	20	350	322.0	0.31
16	5	5	500	135.4	0.11
17	20	5	500	235.2	0.27
18	12.5	12.5	500	191.0	0.19
19	5	20	500	222.5	0.29
20	20	20	500	313.8	0.24

Table 5.6: Regression coefficients and ANOVA estimated for particles size of the nanoemulsions

Source	Sum of Squares	df	Mean Square	F Value	p-value Prob > F	Remarks
Model	2.48E+05	7	35426.61	18.06	<0.0001	Significant
A-Stabilizer	79477.22	1	79477.22	40.51	<0.0001	
B-Oil	36614.6	1	36614.6	18.66	0.001	
C-Pressure	97792.32	1	97792.32	49.84	<0.0001	
AB	8495.56	1	8495.56	4.33	0.0595	
AC	15637.96	1	15637.96	7.97	0.0154	
BC	3982.78	1	3982.78	2.03	0.1797	
A^2	5985.8	12	5985.8	3.05	0.1062	
Residual	2354.41	7	1961.95			
Lack of Fit	19587.2	5	2798.17	3.54	0.0916	Not significant
Pure Error	3956.21	19	791.24			
Cor Total	2.72E+05					
R^2	0.9133					

Table 5.7: Regression coefficients and ANOVA estimated for PDI of the nanoemulsions

Source	Sum of Squares	df	Mean Square	F Value	p-value Prob > F	Remarks
Model	0.192726	7	0.027532	4.486863	0.0114	Significant
A-Stabilizer	0.055652	1	0.055652	9.069387	0.0108	
B-Oil	0.026112	1	0.026112	4.255416	0.0615	
C-Pressure	0.073788	1	0.073788	12.02504	0.0047	
AC	0.02773	1	0.02773	4.519102	0.0550	
BC	0.00177	1	0.00177	0.288472	0.6010	
A^2	0.00679	1	0.00679	1.106484	0.3136	
B^2	0.005363	1	0.005363	0.873963	0.3683	
Residual	0.073634	12	0.006136			
Lack of Fit	0.053141	7	0.007592	1.852188	0.2577	Not significant
Pure Error	0.020494	5	0.004099			
Cor Total	0.266361	19				
R^2	0.7521					

Table 5.8: Desirability values at optimized parameters

Oil content (%)	Stabilizer (%)	Pressure (bar)	Particle size (nm)	PDI	Desirability
6.86	5	257.32	242.0	0.193	0.93
6.95	5	256.50	191.8	0.189	0.93
6.66	5	259.12	191.8	0.190	0.93
6.16	5	263.85	192.5	0.192	0.93

Table 5.9 Validation of optimization conditions of nanoemulsion

Oil (%)	Stabilizer (%)	Pressure (bar)	Predicted		Experimental		R_{dev}(%)		Over all R_{dev}(%)
			Particle size (nm)	PDI	Particle size (nm)	PDI	Particle size (nm)	PDI	
6.95	5	260	191.81	0.18	181.6	0.19	5.62	0.52	3.07

5.3.10. Particle size of Pickering nanoemulsion (PE)

Liu et al. (2023) and Ngwabebhoh et al. (2018) conducted studies on the stabilization of Pickering nanoemulsion using nanocellulose and Tween 80 and reported that nanocellulose and Tween 80 formed thick interfacial membranes that provided better protection against partial coalescence.

Pickering nanoemulsion was prepared in this study using optimized conditions and was stabilized with ACU-10 nanocellulose (average particle size of 99.65 nm and PDI of 0.166) at 0.05%, 0.1%, 0.2% and 0.3% levels. The particle size of Pickering nanoemulsion PN1, PN2, PN3 and PN4 was 193.2 nm, 259.6 nm, 262.2 nm, and 368.1 nm, respectively and PDI value was 0.411, 0.284, 0.311, and 0368, respectively (Table 5.9, Fig. 5.8). Winuprasith and Suphantharika (2015) reported that droplet size of emulsion increases with an increase in the concentration of microfibrillated cellulose, due to high viscosity and poor mixing of emulsion. Also, droplet aggregation occurs because of an increase in nanocellulose concentration. Jiang and Hsieh (2015) reported that droplet size of an emulsion stabilized with holocellulose nanocrystal is concentration dependent and number of droplets increase with higher concentration of holocellulose nanocrystals (from 0.1 to 0.3%). However, the nanocellulose settles down easily in aqueous medium when there is a broad particle size distribution, which may affect the stability of Pickering nanoemulsion when stabilized with such nanocellulose. In general, van der Waals forces, electrostatic contacts, hydrophobic interactions, and hydrogen bonds all affect Brownian motion in solutions, which stops nanocellulose from moving downward (Niu et al., 2017). In our samples, though the particle size of Pickering nanoemulsion ranged from 193.2 nm - 368.1 nm, the PDI was < 0.4, which may delay the destabilization caused by Ostwald ripening, particularly in PN2 that had the lowest PDI value. Researchers have reported the particle size of Pickering nanoemulsion stabilized with solid particles like cellulose nanocrystal and walnut protein isolates to range from 14 – 34 μm (Mikulcová et al., 2016) and 3.07–8.95 μm (Liu et al., 2023), respectively. Liu et al. (2023)

reported that nanoparticle size may have a direct impact on Pickering emulsion stability, and smaller particles may increase solid particle adsorption capacity at the interface. Zhao et al. (2020) stabilized Pickering emulsion with zein nanoparticles and Tween 20 having particle size varying from 73.52 - 300.4 nm and PDI value within 0.2. The authors considered their emulsion to be homogenous and monodisperse dispersion without significant aggregation.

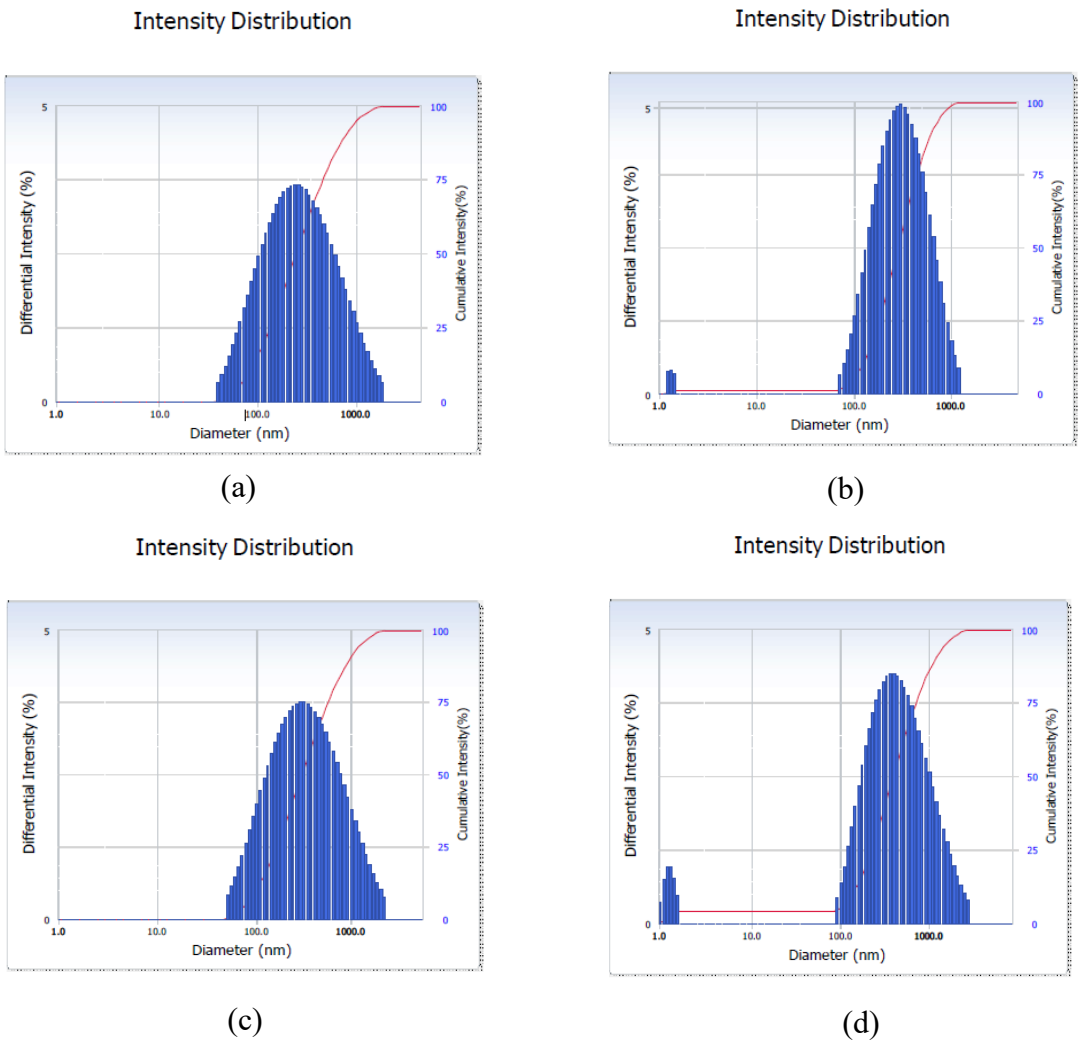

Fig. 5.8. Particle size and PDI value of curcumin-enriched Pickering nanoemulsions (a) PN1, (b) PN2, (c) PN3, and (d) PN4.

Table 5.10. Particle size and PDI value of curcumin-enriched Pickering nanoemulsions

Samples	Particle size (nm)	Polydispersity index
PN1	193.2	0.41
PN2	259.6	0.28
PN3	262.2	0.31
PN4	368.1	0.37

5.3.11. Evaluation of curcumin stability in Pickering nanoemulsion

To overcome the instability of curcumin, the curcumin-enriched Pickering nanoemulsion was prepared and stability of curcumin was analysed at different temperatures and pH levels. The curcumin stability of Pickering nanoemulsion was evaluated after adjusting the pH from 2 to 8 (Table 5.10) and investigated by RP-HPLC for content (Fig. 5.10). The curcumin content of PN1, PN2, PN3, and PN4 decreased with an increase in pH from acidic to alkaline range. The decrease was from 7.78 mg/100 ml to 5.94 mg/100 ml, 8.04 mg/100 ml to 6.74 mg/100 ml, 6.75 mg/100 ml to 5.48 mg/100 ml, and 6.42 mg/100 ml to 5.06 mg/100 ml, respectively. PN2 having 0.1% nanocellulose retained the highest curcumin content in the pH range studied. The curcumin reduction in PN2 was 38.8%, 44.7%, 45.3% and 48.7% at pH 2, 4, 6, and 8, respectively.

Table 5.11. RP-HPLC analysis of curcumin in Pickering nanoemulsion at different pH.

Sample	Retention time	Curcumin content (mg/100 ml)				
		Control	pH 2	pH 4	pH 6	pH 8
PN1	10.26	13.05 ± 0.02^{aA}	7.78 ± 0.08^{bA}	7.04 ± 0.05^{cA}	6.41 ± 0.51^{cdB}	5.94 ± 0.24^{dB}
PN2	10.26	13.15 ± 0.28^{aA}	8.04 ± 0.60^{bA}	7.26 ± 0.18^{cA}	7.29 ± 0.04^{cA}	6.74 ± 0.09^{cA}
PN3	10.26	13.02 ± 0.01^{aA}	6.75 ± 0.09^{bB}	6.64 ± 0.36^{bcB}	6.00 ± 0.07^{cB}	5.48 ± 0.11^{dBC}
PN4	10.26	12.06 ± 0.62^{aA}	6.42 ± 0.29^{bB}	5.45 ± 0.16^{cC}	5.27 ± 0.10^{cC}	5.06 ± 0.04^{cC}

Control- Pickering nanoemulsion without pH treatment

$^{a-d}$ Values with different superscripts vary significantly within a row at $p < 0.05$ and $^{A-C}$Values with different superscripts vary significantly within a column at $p < 0.05$.

Curcumin turns red in colour and occurs in the protonated form (H_4A^+) at pH values >8 and is yellowish and mostly found in the neutral form in 1 to 7 pH solutions (H_3A). Curcumin is more stable in acidic environments and, as a result, more resistant to degradation because of the progressive disintegration of its conjugated diene structure when the proton is removed during the dissociation of phenolic groups in the curcumin structure (HA2-, H2A-, and A3-) at higher pH values (Lee et al., 2013).

The stability of curcumin in two different temperatures were determined and the results are reported in Table 5.11 and Fig. 5.11. The curcumin content in PN1, PN3, and PN4 decreased from 8.27 mg/100 ml to 5.90 mg/100ml at 63℃ and from 6.79 mg/100 ml to 5.22 mg/100 ml at 95 ℃. The curcumin reduction in PN1, PN3, and PN4 at 95 ℃ was 47.6%, 55.2% and 56.7%, respectively and at 63 ℃ was 36.6%, 46.4% and 51%, respectively. A significantly higher curcumin content at 63℃ and 95℃ was observed in PN2 than PN1, PN3, and PN4. PN2 registered curcumin content of 8.81±0.12 mg/100 ml and 8.61±0.27 mg/100 ml at 63℃ and 95℃, respectively. PN2 also had the lowest PDI value as compared to all other Pickering nanoemulsions. PDI describes the uniformity of the sample in suspension. The higher the PDI, the less uniform the sample is. The concentration of nanoparticles plays a crucial role in preventing coalescence and enhancing stability. Aw et al. (2022) reported that the surface coverage of cellulose nanocrystals (CNC) on the droplet interface is poor at low CNC concentrations (i.e., 0.1 to 0.5 g/100 ml), suggesting that the PE is not completely covered by solid particles. Curcumin is transferred more quickly from the oil phase into the aqueous phase when a portion of the oil phase is in contact with curcumin, and this accelerates curcumin degradation. Aw et al. (2022) observed that the curcumin stability decreased at 50 ℃ when the CNC concentration increased from 0.1 g/100 ml to 1.5 g/100 ml, suggesting that the rate of curcumin degradation increases linearly with the increase in CNC concentration. The curcumin reduction in PN2 at 63 ℃ and 95 ℃ was 33% and 34.5%, respectively. Li et la. (2016) reported that curcumin may migrate into hot water due to better water solubility of medium chain triglycerol oil and curcumin at higher temperature, which releases curcumin from nanoemulsion droplets, due to which curcumin faces hydrolyzation and oxidation in the aqueous solution. Similarly, curcumin concentration in Pickering nanoemulsion PN1, PN3, and PN4 decreased at 63 ℃ and 95 ℃, which might be due to their unstable droplets as compared to PN2. In comparison to PN1, PN3, and PN4, the curcumin content retained in PN2 was maximum at the temperatures studied (8.81 mg/100 ml in 63 ℃ and 8.61 mg/100 ml in 95 ℃) with no significant difference, which may be due to its lower particle size and PDI value. A narrow and concentrated particle size and better stability inhibited the curcumin migration

during the thermal treatment of PN2. Higher PDI value and particle size leads to coalescence or Ostwald ripening of nanoemulsion. Wen et al. (2014) reported that CNCs were irreversibly adsorbed to cover emulsion droplets and formed 2 D-network. When the temperature increases, CNC structure becomes stronger and consequently, the inter-particle distances are decreased and the associative forces among the nanocrystals are increased. This explains the non-significant difference of curcumin concentration at 63 ℃ and 95 ℃ in Pickering nanoemulsion stabilized with 0.1% nanocellulose.

Table 5.12. RP-HPLC analysis of curcumin in Pickering nanoemulsion at two different temperatures

Samples	Retention time	Curcumin content (mg/100 ml)		
		Control	63℃	95℃
PN1	10.26	13.05 ± 0.02^{aA}	8.27 ± 0.23^{bB}	6.79 ± 0.54^{cB}
PN2	10.26	13.15 ± 0.28^{aA}	8.81 ± 0.12^{bA}	8.61 ± 0.27^{bA}
PN3	10.26	13.02 ± 0.01^{aA}	6.97 ± 0.45^{bC}	5.82 ± 0.61^{cC}
PN4	10.26	12.06 ± 0.62^{aA}	5.90 ± 0.36^{bD}	5.22 ± 0.12^{bD}

Control: Pickering nanoemulsion without temperature treatment

[a-c] Values with different superscripts vary significantly within a row at p <0.05 and [A-D]Values with different superscripts vary significantly within a column at p <0.05.

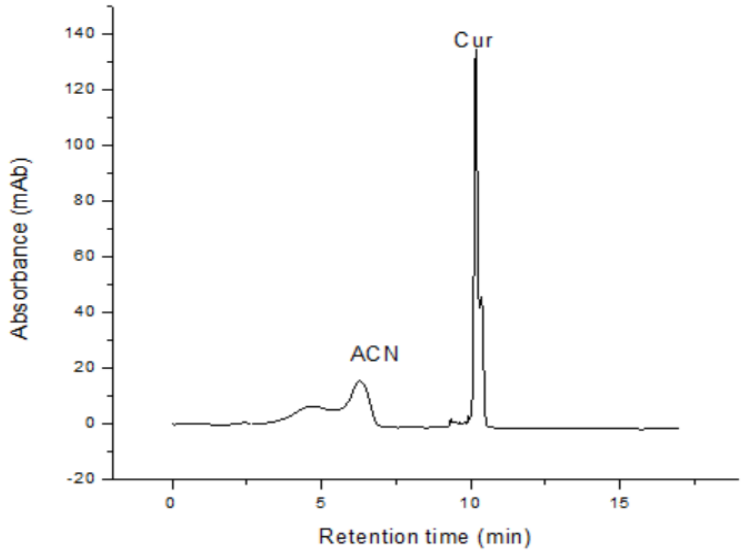

Fig 5.9. RP- HPLC chromatogram of standard curcumin

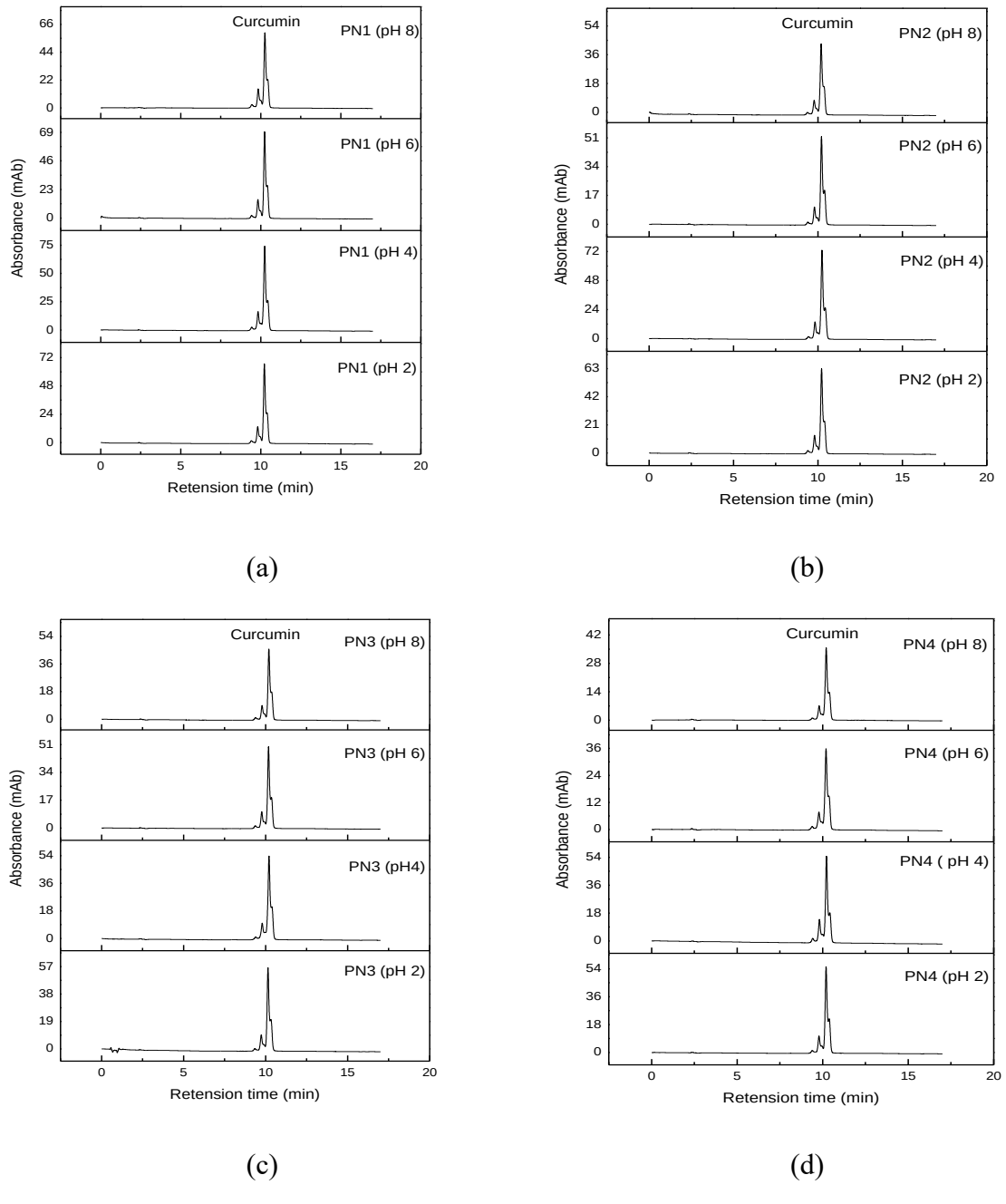

Fig 5.10. RP- HPLC chromatograms showing stability of curcumin content in Pickering nanoemulsions: (a) PN1, (b) PN2, (c) PN3, and (d) PN4 at pH 2, 4, 6, and 8.

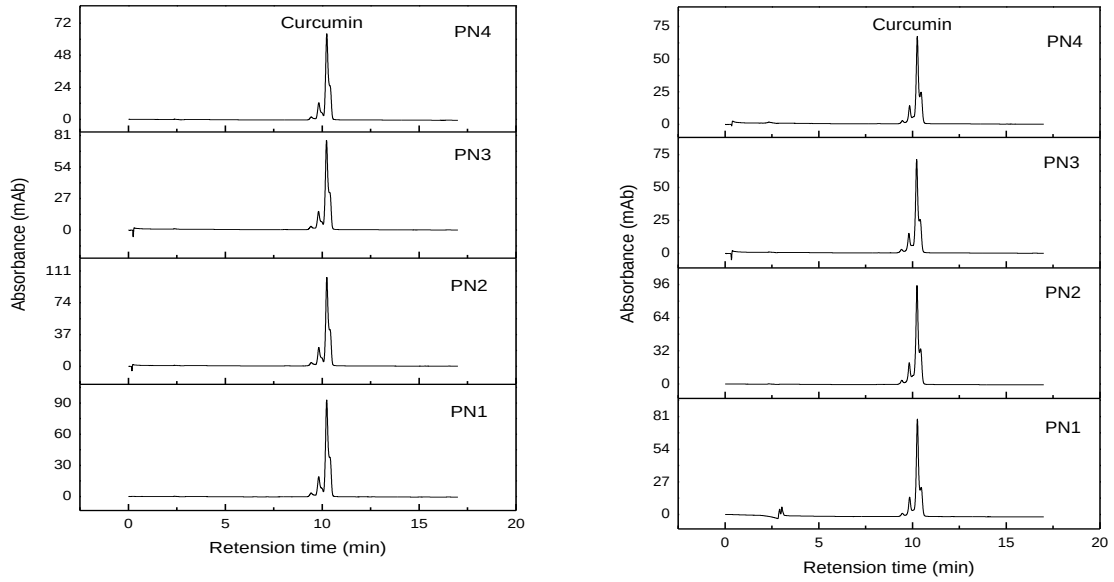

Fig 5.11. RP- HPLC chromatograms showing stability of curcumin in Pickering nanoemulsions (PN1, PN2, PN3 and PN4) at (a) 63 ℃ and (b) 95 ℃.

5.3.12. Creaming index of Pickering nanoemulsion

Stability is commonly addressed by analysing the physical changes in the emulsion over a practical length of time. The percentage creaming index (%CMI) of Control (nanoemulsion without nanocellulose) and Pickering nanoemulsion sample was studied. Fig. 5.12 presents the %CMI of Pickering nanoemulsion over a period of 30 days. The obtained results showed 6.6 %CMI of Control on day 5 of storage at room temperature. On the other hand, PN1, PN3 and PN4 did not show any phase separation until day 5; on day 10, PN4 having 0.3% nanocellulose showed 6% of %CMI but other Pickering nanoemulsions having 0.05%, 0.1% and 0.2% nanocellulose did not show any separation until day 15. The results disclosed that with an increase in the concentration of nanocellulose in the Pickering emulsion, the %CMI also increased; this might be due to the increase in particle size and PDI value of Pickering nanoemulsion. The lowest PDI value of PN2 (Table 5.7) may have prevented separation as compared to the other Pickering nanoemulsions. Researchers have reported that the type of surfactant used had a direct impact on the durability of emulsions (Pengon et al., 2018). PN1, PN3 and PN4 having Tween 80 (5%) and nanocellulose (0.05%, 0.2% and 0.3%) showed creaming index of 6%, 40% and 60% on 30 day of storage at room temperature, while PN2 having 0.1% nanocellulose had 0 %CMI up to day 30. Nanocellulose concentration has been reported to be an important parameter for the stability of Pickering emulsion from coalescence (Ngwabebhoh et al., 2018). Aw et al. (2022) reported that a nanocellulose-stabilized Pickering

emulsion did not require a CNC concentration of more than 1.5 g/100 ml because it formed a very thick, gel-like Pickering emulsion. In contrast, with increase in nanocellulose concentration there is a shift toward larger average particle size of Pickering nanoemulsion. This agrees with the work of Ntazinda et al. (2014), who reported that increasing the carboxymethyl cellulose concentration above a certain level (to 6 g/L) caused a broadening of the particle size peak toward larger sizes. Similarly, in our study, very low or high nanocellulose affected the stability of curcumin-enriched Pickering nanoemulsion. The stability of the nanoemulsified beverages was evaluated based on the increase in their particle size and PDI value of droplets. As the PDI value of the nanocellulose ACU-10 was lower than 0.25, there was uniformity of the sample in suspension. The higher the PDI, the less uniform the sample is. With uniform nanocellulose, better stability of Pickering nanoemulsion is obtained. Danaei et al. (2018) reported that PDI value of 1.0 indicated that the sample has diverse particle sizes. The PDI value of <0.2 or lower is typically considered satisfactory; especially when using lipid-based carriers, the PDI of 0.3 or lower is viewed as desirable. Previous research has highlighted that the structure of emulsions stabilized by CNF consists of droplet aggregates formed through the intertwining and interactions among fibers (Jiménez and Capron, 2018). While these aggregates are more resistant to deformation, they might undergo changes when subjected to deformations beyond a critical point (Jiménez and Capron, 2018). Such alterations in the structure can subsequently impact the release pattern of curcumin from the Pickering nanoemulsion. The concentration of nanoparticles plays a crucial role in preventing coalescence and enhancing stability. In PN1, PN2, PN3 and PN4, when the concentration of nanocellulose was increased from 0.05% to 0.3%, there was an evident rise in particle size. Sari et al. (2015) reported that individual use of Tween 80 (1-10%) and WPC-70 (1-5%) for nanoemulsion preparation did not show a good result with respect to their stability as studied during heating. Among the Pickering nanoemulsions studied, PN2 had the lowest PDI value. PDI describes the uniformity of the sample in suspension. The higher the PDI, the less uniform the sample is. PN1 exhibited cream separation (CMI%) after 30 days in storage, whereas PN2 showed no such separation during the same duration. Even though PN2 had higher particle size, its PDI value being low helped in stabilizing the nanoemulsion. According to Souza et al. (2022), the crystalline planes of cellulose favour their adsorption at the oil/water interface and, consequently, promote the emulsion stability.

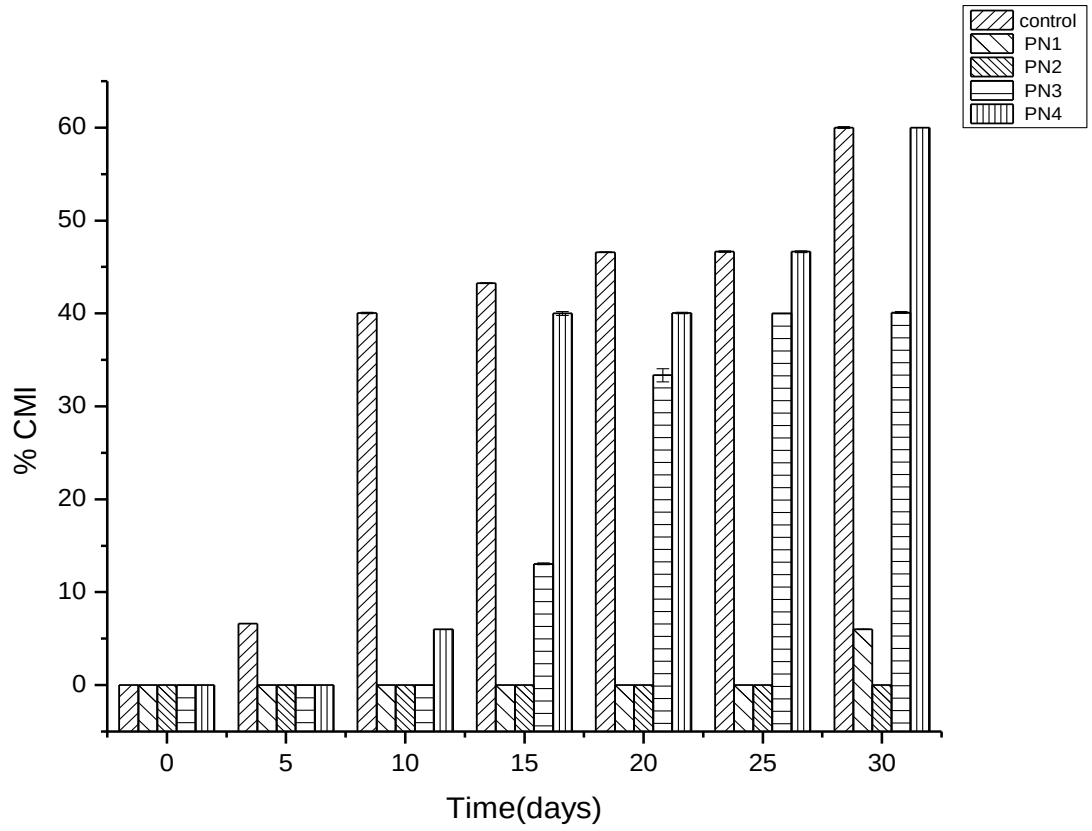

Fig 5.12: Creaming index of Pickering nanoemulsion (PN1, PN2, PN3, and PN4).

5.4. Conclusion

The nanocellulose from coconut milk waste residue that was extracted using low sulphuric acid concentration (42%) and ultrasonication time of 10 min, coded as ACU-10, was able to form a stable Pickering nanoemulsion because of its small particle size and low PDI of 0.166. Combined treatments of acid and ultrasonication developed higher crystallinity and thermal stability in the nanocelluloses, particularly in ACU-10. Moreover, acid treatment along with mechanical treatment enhanced the crystallinity of the nanocellulose. The emission of heat due to cavitation effect leads to bond breakage and further disintegration of the nanocellulose obtained after acid hydrolysis. HPLC results suggested that nanoemulsion stabilized with ACU-10 was able to retain maximum amount of curcumin. Curcumin degradation was lowest in the Pickering emulsion stabilized with 0.1% nanocellulose (sample PN2) at different pH (2-8) and temperature (63^{o}, 95^{o}) levels when compared with other samples due to its better stability and lower PDI value. The results disclosed that with an increase in the concentration of nanocellulose in the Pickering emulsion the %CMI also increased, this might be due to increase in particle size and PDI value of Pickering nanoemulsion. The lowest PDI value (0.28) of PN2 may have prevented separation as compared to other Pickering nanoemulsions. When the

concentration of nanocellulose was increased from 0.05% to 0.3% in the Pickering nanoemulsion, there was an evident rise in particle size. On the basis of the particle size and PDI values of the nanoemulsion droplets, it can be said that PN2 is more stable than PN1, PN3, and PN4. PN2 also exhibited marginal creaming in comparison to PN1, PN3, and PN4. Even though PN2 had higher particle size, its PDI value being low helped in stabilizing the nanoemulsion. The concentration of nanocellulose in the emulsion droplets plays a crucial role in preventing coalescence and enhancing stability.

Bibliography

Aditya, N. P., Aditya, S., Yang, H. J., Kim, H. W., Park, S. O., Lee, J., and Ko, S. (2015). Curcumin and catechin co-loaded water-in-oil-in-water emulsion and its beverage application. *Journal of Functional Foods*, 15:35–43.

Almasi, H., Azizi, S., and Amjadi, S. (2020). Development and characterization of pectin films activated by nanoemulsion and Pickering emulsion stabilized marjoram (Origanum majorana L.) essential oil. *Food Hydrocolloids*, *99*:105338

Alzate-Arbeláez, A. F., Dorta, E., López-Alarcón, C., Cortés, F. B., and Rojano, B. A. (2019). Immobilization of Andean berry (Vaccinium meridionale) polyphenols on nanocellulose isolated from banana residues: A natural food additive with antioxidant properties. *Food Chemistry*, *294*:503–517.

Andresen, M., Johansson, L. S., Tanem, B. S., and Stenius, P. (2006). Properties and characterization of hydrophobized microfibrillated cellulose. *Cellulose*, *13*(6), 665–677.

Asabuwa Ngwabebhoh, F., Ilkar Erdagi, S., and Yildiz, U. (2018). Pickering emulsions stabilized nanocellulosic-based nanoparticles for coumarin and curcumin nanoencapsulations: In vitro release, anticancer and antimicrobial activities. *Carbohydrate Polymers*, *201*:317–328.

Asem, M., Noraini Jimat, D., Huda Syazwani Jafri, N., Mohd Fazli Wan Nawawi, W., Fadhillah Mohamed Azmin, N., and Firdaus Abd Wahab, M. (2023). Entangled cellulose nanofibers produced from sugarcane bagasse via alkaline treatment, mild acid hydrolysis assisted with ultrasonication. *Journal of King Saud University - Engineering Sciences*, *35*(1):24–31.

Cao, Y., Zavattieri, P., Youngblood, J., Moon, R., and Weiss, J. (2016). The relationship between cellulose nanocrystal dispersion and strength. *Construction and Building Materials*, *119*:71–79.

Choi, S. J., and McClements, D. J. (2020). Nanoemulsions as delivery systems for lipophilic nutraceuticals: Strategies for improving their formulation, stability, functionality and bioavailability. *Food Science and Biotechnology*, *29*:149–168.

Chutia, H., and Mahanta, C. L. (2021). Properties of starch nanoparticle obtained by ultrasonication and high-pressure homogenization for developing carotenoids-enriched powder and Pickering nanoemulsion. *Innovative Food Science and Emerging Technologies*, 74:102822.

Danaei, M. R. M. M., Dehghankhold, M., Ataei, S., Hasanzadeh Davarani, F., Javanmard, R., Dokhani, A., and Mozafari, M. R. (2018). Impact of particle size and polydispersity index on the clinical applications of lipidic nanocarrier systems. *Pharmaceutics*, *10*(2):57.

Ding, Y., and Kan, J. (2017). Optimization and characterization of high-pressure homogenization produced chemically modified starch nanoparticles. *Journal of Food Science and Technology*, *54*:4501–4509.

Erdagi, S. I., Ngwabebhoh, F. A., and Yildiz, U. (2020). Pickering stabilized nanocellulose-alginate: A diosgenin-mediated delivery of quinalizarin as a potent cyto-inhibitor in human lung/breast cancer cell lines. *Materials Science and Engineering*, 109:110621.

Foo, M. L., Ooi, C. W., Tan, K. W., and Chew, I. M. (2022). Preparation of black cumin seed oil Pickering nanoemulsion with enhanced stability and antioxidant potential using nanocrystalline cellulose from oil palm empty fruit bunch. *Chemosphere*, *287*:132108.

Gani, A., and Benjakul, S. (2018). Impact of virgin coconut oil nanoemulsion on properties of croaker surimi gel. *Food Hydrocolloids*, *82*:34–44.

Guo, Z., Li, Z., Wang, J., and Zheng, B. (2019). Gelation properties and thermal gelling mechanism of golden threadfin bream myosin containing CaCl2 induced by high pressure processing. *Food Hydrocolloids*, *95*:43–52.

Harini, K., Ramya, K., and Sukumar, M. (2018). Extraction of nano cellulose fibers from the banana peel and bract for production of acetyl and lauroyl cellulose. *Carbohydrate Polymers*, *201*:329–339.

Ishak, N. A. M., Khalil, I., Abdullah, F. Z., and Julkapli, N. M. (2020). A correlation on ultrasonication with nanocrystalline cellulose characteristics. *Carbohydrate Polymers*, 246:116553.

Jiang, F., and Hsieh, Y. L. (2015). Holocellulose nanocrystals: amphiphilicity, oil/water emulsion, and self-assembly. *Biomacromolecules*, *16*(4):1433–1441.

Jiménez Saelices, C., and Capron, I. (2018). Design of Pickering Micro- and Nanoemulsions Based on the Structural Characteristics of Nanocelluloses. *Biomacromolecules*, *19*(2):460–469.

Joung, H. J., Choi, M. J., Kim, J. T., Park, S. H., Park, H. J., and Shin, G. H. (2016). Development of food-grade curcumin nanoemulsion and its potential application to food beverage system: antioxidant property and in vitro digestion. *Journal of Food Science*, *81*(3):745–N753.

Kamel, R., El-Wakil, N. A., Dufresne, A., and Elkasabgy, N. A. (2020). Nanocellulose: From an agricultural waste to a valuable pharmaceutical ingredient. *International Journal of Biological Macromolecules*, *163*:1579–1590.

Kanchanathawornviboon, X., Monton, C., and Urairong, H. (2021). Microwave-assisted extraction of curcuminoids from organic Curcuma longa L. in different oil types for cosmetic purpose: An optimization approach. *Journal of Current Science and Technology*, *11*(1):71–89.

Kassab, Z., El Achaby, M., Tamraoui, Y., Sehaqui, H., Bouhfid, R., and Qaiss, A. E. K. (2019). Sunflower oil cake-derived cellulose nanocrystals: Extraction, physico-chemical characteristics and potential application. *International Journal of Biological Macromolecules*, *136*:241–252.

Keshavamurthysetty, P. H., and Patel, D. H. (2023). Effect of Process Variables on the Development and Characterization of Nanocellulose as Novel Biopolymer. *Indian Journal of Pharmaceutical Education and Research*, *57*(1):32–s40.

Kharat, M., Du, Z., Zhang, G., and McClements, D. J. (2017). Physical and Chemical Stability of Curcumin in Aqueous Solutions and Emulsions: Impact of pH, Temperature, and Molecular Environment. *Journal of Agricultural and Food Chemistry*, *65*(8):1525–1532.

Lavanya, D. K. P. K., Kulkarni, P. K., Dixit, M., Raavi, P. K., and Krishna, L. N. V. (2011). Sources of cellulose and their applications—A review. *International Journal of Drug Formulation and Research*, *2*(6):19–38.

Lee, W. H., Loo, C. Y., Bebawy, M., Luk, F., Mason, R. S., and Rohanizadeh, R. (2013). Curcumin and its derivatives: their application in neuropharmacology and neuroscience in the 21st century. *Current Neuropharmacology*, *11*(4):338–378.

Li, J., Hwang, I. C., Chen, X., and Park, H. J. (2016). Effects of chitosan coating on curcumin loaded nano-emulsion: Study on stability and in vitro digestibility. *Food Hydrocolloids*, *60*:138–147.

Liu, J., Zhang, H., Sun, X., and Fan, F. (2023). Development and characterization of Pickering emulsion stabilized by walnut protein isolate nanoparticles. *Molecules*, *28*(14):5434.

Lu, P. S., Inbaraj, B. S., and Chen, B. H. (2018). Determination of oral bioavailability of curcuminoid dispersions and nanoemulsions prepared from Curcuma longa Linnaeus. *Journal of the Science of Food and Agriculture*, *98*(1):51–63.

Maiti, S., Jayaramudu, J., Das, K., Reddy, S. M., Sadiku, R., Ray, S. S., and Liu, D. (2013). Preparation and characterization of nano-cellulose with new shape from different precursor. *Carbohydrate Polymers*, *98*(1):562–567.

Mandal, A., and Chakrabarty, D. (2011). Isolation of nanocellulose from waste sugarcane bagasse (SCB) and its characterization. *Carbohydrate Polymers*, *86*(3):1291–1299.

Mansora, A. M., Lima, J. S., Anib, F. N., Hashima, H., and Hoa, W. S. (2019). Characteristics of cellulose, hemicellulose and lignin of MD2 pineapple biomass. *Chemical Eng*ineering *72*(1), 79-84.

Mariño, M., Lopes da Silva, L., Durán, N., and Tasic, L. (2015). Enhanced materials from nature: nanocellulose from citrus waste. *Molecules*, *20*(4):5908–5923.

Mikulcová, V., Bordes, R., and Kašpárková, V. (2016). On the preparation and antibacterial activity of emulsions stabilized with nanocellulose particles. *Food Hydrocolloids*, 61:780–792.

Mohd Zin, N. B., Mohamad Yusof, B., Oslan, S. N., Wasoh, H., Tan, J. S., Ariff, A. B., and Halim, M. (2017). Utilization of acid pre-treated coconut dregs as a substrate for production of detergent compatible lipase by Bacillus stratosphericus. *AMB Express*, 7:1–13.

Morán, J. I., Alvarez, V. A., Cyras, V. P., and Vázquez, A. (2008a). Extraction of cellulose and preparation of nanocellulose from sisal fibers. *Cellulose*, *15*(1):149–159.

Nasir, N. A. M. M., Ball, Z., Jalaluddin, A. A., Shadan, I. A., and Abd Manan, *N. E. W.* (2018). Virgin coconut oil and its antimicrobial properties against pathogenic microorganisms: a review. In *International dental conference of sumatera utara*, 192–199. Atlantis Press.

Ng, S. P., Tan, C. P., Lai, O. M., Long, K., and Mirhosseini, H. (2010). Extraction and characterization of dietary fiber from coconut residue. *Journal of Food, Agriculture & Environment*, 2:172–177

Ngwabebhoh, F. A., Erdem, A., and Yildiz, U. (2018). A design optimization study on synthesized nanocrystalline cellulose, evaluation and surface modification as a potential biomaterial for prospective biomedical applications. *International Journal of Biological Macromolecules*, *114*:536–546.

Niu, F., Li, M., Huang, Q., Zhang, X., Pan, W., Yang, J., and Li, J. (2017). The characteristic and dispersion stability of nanocellulose produced by mixed acid hydrolysis and ultrasonic assistance. *Carbohydrate Polymers*, *165*:197–204.

Pengon, S., Chinatangkul, N., Limmatvapirat, C., and Limmatvapirat, S. (2018). The effect of surfactant on the physical properties of coconut oil nanoemulsions. *Asian Journal of Pharmaceutical Sciences*, *13*(5):409–414.

Phanthong, P., Guan, G., Ma, Y., Hao, X., & Abudula, A. (2016). Effect of ball milling on the production of nanocellulose using mild acid hydrolysis method. *Journal of the Taiwan Institute of Chemical Engineers*, *60*:617–622.

Raghavendra, S. N., & Raghavarao, K. S. M. S. (2010). Effect of different treatments for the destabilization of coconut milk emulsion. *Journal of Food Engineering*, *97*(3):341–347.

Rashid, E. S. A., Gul, A., Yehya, W. A. H., and Julkapli, N. M. (2021). Physico-chemical characteristics of nanocellulose at the variation of catalytic hydrolysis process. *Heliyon*, *7*(6).

Romanski, F. S., Jayjock, E., Muzzio, F. J., and Tomassone, M. S. (2011). Important factors in the size reduction of polymer-stabilized drug particle suspensions using high-pressure homogenization. *Journal of Pharmaceutical Innovation*, *6*(2):97–106.

Santmartí, A., and Lee, K.-Y. (2018). Crystallinity and Thermal Stability of Nanocellulose. In *Nanocellulose and Sustainability* (pp. 67–86). CRC Press.

Sari, T. P., Mann, B., Kumar, R., Singh, R. R. B., Sharma, R., Bhardwaj, M., and Athira, S. (2015). Preparation and characterization of nanoemulsion encapsulating curcumin. *Food Hydrocolloids*, *43*:540–546.

Shahabi-Ghahfarrokhi, I., Khodaiyan, F., Mousavi, M., and Yousefi, H. (2015). Preparation and characterization of nanocellulose from beer industrial residues using acid hydrolysis/ultrasound. *Fibers and Polymers*, *16*(3):529–536.

Souza, A. G., Ferreira, R. R., de Oliveira, E. R., Kato, M. M., Mitra, S. K., and Rosa, D. dos S. (2022). Chemical Stabilization behind Cardamom Pickering Emulsion Using Nanocellulose. *Polysaccharides*, *3*(1):200–216.

Sumesh, K. R., Kanthavel, K., and Kavimani, V. (2020). Peanut oil cake-derived cellulose fiber: Extraction, application of mechanical and thermal properties in pineapple/flax natural fiber composites. *International Journal of Biological Macromolecules*, *150*:775–785.

Tang, C., Chen, Y., Luo, J., Low, M. Y., Shi, Z., Tang, J., Zhang, Z., Peng, B., and Tam, K. C. (2019). Pickering emulsions stabilized by hydrophobically modified nanocellulose containing various structural characteristics. *Cellulose*, *26*(13–14):7753–7767.

Tang, Y., Yang, S., Zhang, N., and Zhang, J. (2014). Preparation and characterization of nanocrystalline cellulose via low-intensity ultrasonic-assisted sulfuric acid hydrolysis. *Cellulose*, *21*(1):335–346.

Tangsuphoom, N., and Coupland, J. N. (2008). Effect of pH and ionic strength on the physicochemical properties of coconut milk emulsions. *Journal of Food Science*, *73*(6): E274–E280.

Tikekar, R. V., Pan, Y., and Nitin, N. (2013). Fate of curcumin encapsulated in silica nanoparticle stabilized Pickering emulsion during storage and simulated digestion. *Food Research International*, *51*(1):370–377.

Wang, B., Li, D., Wang, L. jun, Chiu, Y. L., Chen, X. D., and Mao, Z. huai. (2008). Effect of high-pressure homogenization on the structure and thermal properties of maize starch. *Journal of Food Engineering*, *87*(3):436–444.

Wang, X. S., Tang, C. H., Li, B. S., Yang, X. Q., Li, L., and Ma, C. Y. (2008). Effects of high-pressure treatment on some physicochemical and functional properties of soy protein isolates. *Food Hydrocolloids*, *22*(4):560–567.

Wen, C., Yuan, Q., Liang, H., and Vriesekoop, F. (2014). Preparation and stabilization of d-limonene Pickering emulsions by cellulose nanocrystals. *Carbohydrate Polymers*, *112*:695–700.

Winuprasith, T., and Suphantharika, M. (2015). Properties and stability of oil-in-water emulsions stabilized by microfibrillated cellulose from mangosteen rind. *Food Hydrocolloids*, *43*:690–699.

Wulandari, W. T., Rochliadi, A., and Arcana, I. M. (2016). Nanocellulose prepared by acid hydrolysis of isolated cellulose from sugarcane bagasse. In *IOP conference series: Materials Science and Engineering* (Vol. 107:1–012045). IOP Publishing.

Yang, X., Han, F., Xu, C., Jiang, S., Huang, L., Liu, L., and Xia, Z. (2017a). Effects of preparation methods on the morphology and properties of nanocellulose (NC) extracted from corn husk. *Industrial Crops and Products*, *109*:241–247.

Yuan, Y., Gao, Y., Zhao, J., and Mao, L. (2008). Characterization and stability evaluation of β-carotene nanoemulsions prepared by high pressure homogenization under various emulsifying conditions. *Food Research International*, *41*(1):61–68.

Zhang, H., Pang, H., Shi, J., Fu, T., and Liao, B. (2012). Investigation of liquefied wood residues based on cellulose, hemicellulose, and lignin. *Journal of Applied Polymer Science*, *123*(2):850–856.

Zhao, Z., Wang, W., Xiao, J., Chen, Y., and Cao, Y. (2020). Interfacial engineering of pickering emulsion co-stabilized by zein nanoparticles and tween 20: Effects of the particle size on the interfacial concentration of gallic acid and the oxidative stability. *Nanomaterials*, *10*(6): 1068.

Zheng, H., and Lu, H. (2011). Use of kinetic, Weibull and PLSR models to predict the retention of ascorbic acid, total phenols and antioxidant activity during storage of pasteurized pineapple juice. *LWT- Food Science and Technology*, *44*(5):1273–1281.

Zhou, H., Zheng, B., & McClements, D. J. (2021). Encapsulation of lipophilic polyphenols in plant-based nanoemulsions: Impact of carrier oil on lipid digestion and curcumin, resveratrol and quercetin bioaccessibility. *Food & Function*, *12*(8):3420–3432.